

## Elasticity measurements on minerals: a review

ROSS J. ANGEL<sup>1,\*</sup>, JENNIFER M. JACKSON<sup>2</sup>, HANS J. REICHMANN<sup>3</sup> and SERGIO SPEZIALE<sup>3</sup>

<sup>1</sup> Virginia Tech Crystallography Laboratory, Department of Geosciences, Virginia Tech, Blacksburg, VA 24060, USA

\*Corresponding author, e-mail: [rangel@vt.edu](mailto:rangel@vt.edu)

<sup>2</sup> Seismological Laboratory, Division of Geological and Planetary Sciences, California Institute of Technology, Pasadena, CA 91125, USA

<sup>3</sup> Deutsches Geoforschungszentrum, 14473 Potsdam, Germany

**Abstract:** The elasticity of minerals is central to our understanding of the structure and properties of the Earth, and other planets. In the last half-century, and in particular within the last 15 years, there have been many new developments in the experimental methods used to determine the elastic properties of minerals. Not only have new techniques become available, but the pressure and temperature ranges over which they can be applied have been greatly extended and the precision and accuracy of the results have been significantly improved. Given these rapid advances in measurement techniques we provide a brief guide to the theory of the elasticity of minerals, and we review and compare the physical principles and the capabilities of the experimental techniques now available.

**Key-words:** elasticity, elastic tensor, inelastic scattering, Brillouin scattering, ultrasonics.

### 1. Introduction

Elasticity is a material property that is central to our understanding of the structure and properties of the Earth, and other planets. At the planetary scale, the most important information that we have on the Earth's interior below the crust comes from the measurement of seismic wave velocities. Seismic waves are elastic waves, and their velocities in rocks can be calculated from knowledge of the full elastic properties of the minerals, together with models as to how the mineral grains are assembled in to a rock. Elasticity is thus the key item of information that allows us to interpret seismic data in terms of mineral assemblages present in the deep Earth. Elasticity also provides a second probe in to the Earth's interior because it is also directly related to how the volume (and thus density) of a mineral varies with pressure – its Equation of State (EoS). Measurements of equations of state of minerals underpin all of the thermodynamic databases used in petrology to interpret the phase assemblages in rocks. On the microscopic scale, the elastic response of a crystal is related to the second derivative of the free energy of the crystal with respect to reversible physical deformation. The elasticity of crystals is thus a very sensitive probe of the interactions and forces between atoms that govern the structure and stability of minerals. This relationship is particularly accentuated in the neighbourhood of phase transitions, where it provides the most sensitive test of physical theories of phase transitions (Carpenter & Salje, 1998; Carpenter, 2006).

It is now over 50 years since the classic text on crystal physics was published (Nye, 1957), in which the tensor

description of the physical properties of crystals was clearly laid out. The book remains the fundamental text book for workers in the field of mineral physics, and especially in elasticity, because the basic theory of single-crystal elasticity is essentially complete. But in the ensuing half-century, there have been many new developments in the experimental measurement of elasticity, in the range of available techniques, the pressure and temperature ranges accessible, and the precision and accuracy of the results. In particular, the developments have been quite remarkable over the last decade and a half. Much of this development has been driven by the need for accurate determinations of elastic properties (and thus seismic wave velocities) in order to interpret the ever-increasing resolution and accuracy of the seismic images of the interior of our planet. As an example, we show in Fig. 1 the development of the measurements of the room-pressure bulk modulus of magnesium silicate perovskite with time. It should be noted that, for the most part, earlier measurements were not wrong, but that the data scatter was greater than would be expected from error estimates. This sort of variation drove many experimental groups to improve the measurement techniques and to explore and eliminate the sources of systematic error in measurements, and at the same time to explore the accuracy of pressure scales that underlay many of these measurements. Some of the earlier data scatter, as in other minerals, can now be understood as being due to minor variations in chemistry and physical state between different samples. As one can see (Fig. 1) modern measurements with very different techniques have converged to mutual agreement within

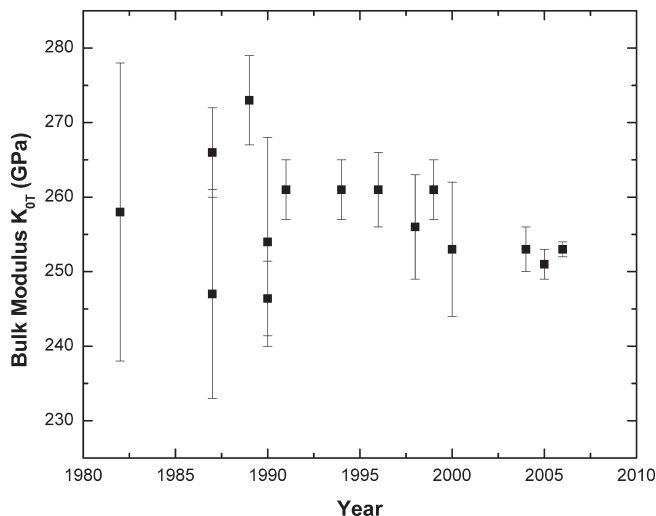


Fig. 1. Experimentally-determined values of the bulk modulus of pure  $\text{MgSiO}_3$  perovskite plotted by year of publication. Note the recent convergence of values from Brillouin spectroscopy (Sinogeikin *et al.*, 2004b), ultrasonic interferometry (Li and Zhang, 2005), and X-ray diffraction (Vanpeteghem *et al.*, 2006).

the much-reduced uncertainties of the individual methods. The same is true for other minerals. Modern precision and accuracy now allows one to explore subtle variations in elasticity that may arise from chemical substitutions, phase transitions, or simple variations with temperature and pressure. The development of new technologies, and the improvement of established ones, now also allows the measurement of elastic properties over the temperature and pressure range from the Earth's crust to its core. And the mutual agreement between different methods allows one to select the experimental technique that is best suited for the available samples and scientific question, with confidence that accurate and precise results will be obtained.

Given these rapid advances in measurement techniques, it is the purpose of this review to present a brief guide to both the theory of the elasticity of minerals, which draws heavily on Nye (1957), and a summary of the physical principles and the capabilities of each of the experimental techniques now available.

## 2. Elasticity basics

In this section we introduce the fundamental concepts of elasticity; stress, strain, and the relationship between them expressed as the elastic properties of materials. This section only provides a brief overview of the subject, so the reader is directed to Chapters V, VI and VIII of Nye (1957) for a comprehensive and definitive explanation of these topics.

### 2.1. Fundamental concepts

The elastic properties of a material define how the material deforms, or changes shape, as a result of forces applied to a body made up of the material. Elasticity specifically only

refers to reversible and instantaneous changes; it does not include time-dependent deformation (anelasticity) nor permanent and irreversible changes (plastic deformation). In more formal language, the forces applied to a body are defined as “stresses” and the resulting elastic deformations are described as “strains”. The elastic properties of a material therefore relate stresses and the resulting strains. This relationship can be most easily illustrated by considering the response of a material such as a mineral to an increase in the external pressure applied to the crystal. In this case, the applied stress is the increase in pressure,  $\Delta P$ . As a consequence of the increase in pressure, the volume of the crystal decreases by an amount  $\Delta V$ . The magnitude of the volume change depends on the size of the crystal; a crystal of twice the volume of another of the same material will exhibit a volume change  $\Delta V$  that is also twice as large. Therefore, in order for the material property of elasticity to be independent of the size of the sample considered, the strain is defined in this case as the fractional change in volume  $\Delta V/V$ . The relationship between the stress,  $\Delta P$ , and the resulting strain  $\Delta V/V$  can then be expressed in one of two ways. The natural way is to express the strain as the result of the applied stress:  $\Delta V/V = f(\Delta P)$ . For small increments in stress, we can assume that the relationship between stress and strain is linear, and write this as  $\Delta V/V = -\beta \Delta P$ . The coefficient  $\beta$  is a property of the material that measures its *softness*; the larger the value of  $\beta$ , the larger the fractional decrease in the volume for a given increase in pressure. In the language of elasticity theory, “softness” coefficients such as  $\beta$  are termed “compressibilities” (when applied to volume) or more generally “compliances”. A compliant material, *i.e.* one with large compliances, is therefore soft. The relationship between volume strain and pressure can also be inverted;  $\Delta P = (-1/\beta)(\Delta V/V)$  and then rewritten as  $\Delta P = -K(\Delta V/V)$ , where  $K = -1/\beta$ . The coefficient  $K$  now represents the “stiffness” of the material, because larger values mean that a given pressure increase results in a smaller change in volume, or smaller strain. Coefficients such as  $K$  are termed “moduli”, singular “modulus”. At this point we should note that the language of elasticity has evolved over the past half-century, and care should be taken in reading older papers as the term “modulus” was originally used as a synonym for “compliance” in the English literature. The correct interpretation, however, can be always unambiguously determined from the units of the elastic property. Dimensional analysis of the equations we have introduced above shows that moduli have units of pressure, such as GPa, bars or dyne  $\text{cm}^{-2}$ , and compliances have units of inverse pressure, such as  $\text{GPa}^{-1}$ . Nye (1957), in the introduction to his chapter on elasticity, provides a glossary of such terms as were then in use.

The relationships that we have introduced above between pressure increase and fractional volume change (*i.e.*, stress and strain) are linear. This means that the resulting strain is proportional to the applied stress, an example of Hooke's Law. While this is not always the case for large stresses, for example when large changes in hydrostatic pressure are applied to a crystal, the majority

of the measurement techniques described in this review apply small stresses and we will therefore normally only be concerned with the Hooke's Law regime.

## 2.2. Stress

We have introduced the concept of stress as a force applied to a body of material, with the specific example of hydrostatic pressure. However, the applied forces do not have to be equal in all directions, so the concept of stress has to handle the variation with direction of the applied force. Stress is therefore not a single number such as pressure, but a *second rank tensor* (Nye, 1957), and the description of stress requires the use of a reference coordinate system, or axes. For all tensor properties it is convenient to use a Cartesian reference system of three mutually perpendicular axes  $X$ ,  $Y$ , and  $Z$ , of unit length. Now consider a cube of material (Fig. 2) oriented with its faces perpendicular to the reference axes. There are two types of force that can be applied to the surface of the cube. The *normal* forces are the three forces applied along the axes, perpendicular to the faces of the cube. They may be compressive (squashing the cube) or extensional (stretching the cube). The normal stress applied to the face perpendicular to the  $X$  axis is then denoted as  $\sigma_{11}$ , and is defined as the force divided by the area of the face. Normal stresses therefore have the units of pressure. Similarly (Fig. 2) the normal stresses along the  $Y$  and  $Z$  axes are denoted as  $\sigma_{22}$  and  $\sigma_{33}$  respectively. The convention (Nye, 1957, Chapter V) is that compressive stresses are given negative values, and tensional stresses positive values. In addition, there may also be shear forces applied to the faces of the cube. A force in the direction of  $+X$  applied to the face perpendicular to the  $Y$  axis gives rise to a positive shear stress  $\sigma_{12}$ , again equal to the force divided by the area of the face. A shear stress in

the opposite direction (*i.e.*, towards  $-X$ ) on the same face would have a negative value of  $\sigma_{12}$ . A shear stress on the same face perpendicular to the  $Y$  axis in the direction of the  $+Z$  axis is denoted  $\sigma_{32}$ . Given that there are six faces on a cube, and three stresses (one normal and two shear) that can be applied to each face, it appears that there can be a total of 18 stresses. However, if we assume that the stress field in the body is equal at every point (*i.e.*, homogeneous), then it follows that the forces on the pairs of opposite faces of the cube must be equal. This reduces the number of stresses from 18 to 9. We also assume that the cube is in static equilibrium, which means that there are no net torques, or rotational forces. Therefore pairs of shear components such as  $\sigma_{12}$  and  $\sigma_{21}$  are equal, and there are thus only six independent components of the stress tensor.

## 2.3. Tensor notation

In this review we will sometimes wish to refer to a specific component of the stress, such as  $\sigma_{21}$ . At other times we will need to refer to the stress tensor with its six independent components as a whole. For this we introduce general suffixes, so that the stress tensor is written as  $\sigma_{ij}$ , with the values of  $i$  and  $j$  each being able to take the values of 1, 2, or 3. The symbol  $\sigma_{ij}$  then represents the total of  $3 \times 3 = 9$  tensor components of which the three pairs of shear components are equal;  $\sigma_{ij} = \sigma_{ji}$ . The same suffix notation, and their range of values, will apply to all tensors discussed in this review.

## 2.4. Strain

Strain is also a second rank tensor, and the description of strains follows exactly the same conventions as that for the stress tensor, and is described with reference to the same Cartesian coordinate system. The change in shape of a unit cube (Fig. 3) can be broken down into a combination of changes in length of the cube along the  $X$ ,  $Y$ , and  $Z$  axes, and changes in the angles (shears) between them. The linear strains along the  $X$ ,  $Y$ , and  $Z$  axes are simply the fractional change in length along these directions. If we draw a line along the  $X$  axis of length  $x$  before the deformation is imposed, and it changes by  $\Delta x$ , then the normal strain along  $X$  is denoted  $\epsilon_{11} = \Delta x/x$ . Note that a decrease in length, or compression, results in negative normal strains. The shear strain  $\epsilon_{12}$  describes the change in the shape of the face of the cube that was originally parallel to the  $X$  and  $Y$  axes, *i.e.* the face of the cube perpendicular to the  $Z$  axis. Formally, if two lines are drawn on this face parallel to the  $+X$  and  $+Y$  axes, they will be perpendicular to one another before the deformation. After an infinitesimal strain of  $\epsilon_{12}$  the angle between them will be  $90^\circ - 2\epsilon_{12}$  (Fig. 3). In the treatment of elasticity and the resulting strains, we do not have to consider any bulk rotations of the sample cube (see Nye, 1957, chapter VI). As a consequence, the strain tensor becomes symmetric with  $\epsilon_{ij} = \epsilon_{ji}$ , and has only six independent components.

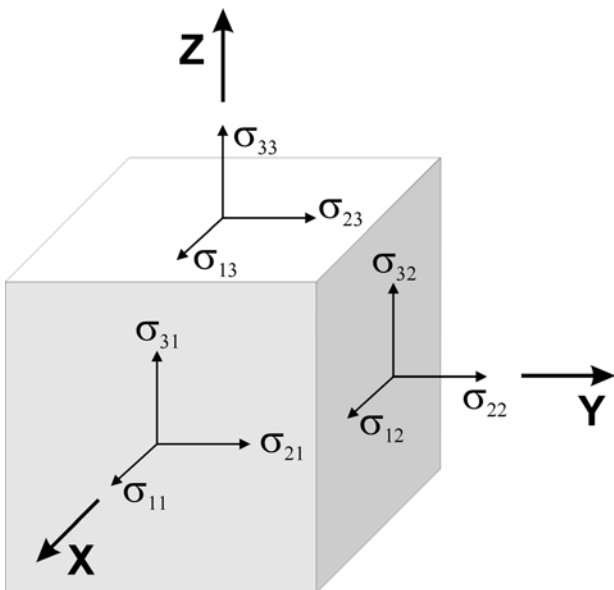


Fig. 2. The definitions of forces on the face of a cube with respect to a set of Cartesian reference axes  $X$ ,  $Y$  and  $Z$ .

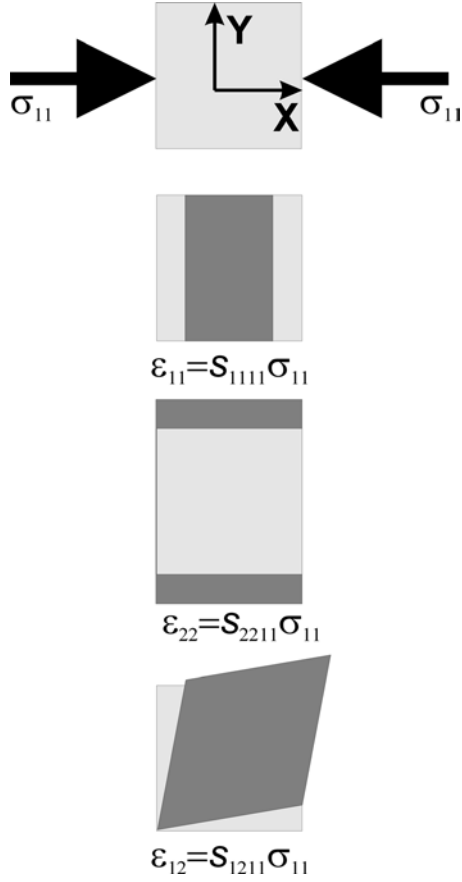


Fig. 3. An illustration of the meaning of the individual components of the compliance tensor  $s_{ijkl}$  in terms of the deformation of a material due to an applied stress  $\sigma_{11}$ . The darker shape represents a single component of the strain relative to the undeformed shape shown in a lighter shade.

## 2.5. Compliance tensor

Because stress and strain are tensor properties, each with nine components, the elastic properties of a material are also described by a tensor that must have  $9 \times 9 = 81$  components in order to be able to relate each stress component to each strain component. Such a tensor is the compliance tensor  $s_{ijkl}$ , which specifies the strains resulting from an applied stress as  $\varepsilon_{ij} = s_{ijkl}\sigma_{kl}$ . The meaning of this compact notation, that represents nine equations each containing nine terms, is best made clear by writing out the equation for just one of the strains, such as  $\varepsilon_{12}$ ;

$$\begin{aligned} \varepsilon_{12} = & s_{1211}\sigma_{11} + s_{1212}\sigma_{12} + s_{1213}\sigma_{13} \\ & + s_{1221}\sigma_{21} + s_{1222}\sigma_{22} + s_{1223}\sigma_{23} \\ & + s_{1231}\sigma_{31} + s_{1232}\sigma_{32} + s_{1233}\sigma_{33} \end{aligned} \quad (1)$$

In expanding  $\varepsilon_{ij} = s_{ijkl}\sigma_{kl}$ , we have chosen the values of  $i$  and  $j$  to define the component of the strain in which we are interested ( $i = 1$  and  $j = 2$ ). The remainder of the expansion is performed by allowing the *dummy suffixes*  $k$  and  $l$  to take all possible allowed values (*i.e.*, from 1 to 3) and

summing all of the resulting terms. We see immediately from this expansion that each of the components of strain depends upon all nine components of the stress tensor.

The significance of the individual components of the compliance tensor can be understood by considering the various strains arising from a single compressive stress applied along the  $X$  axis (Fig. 3). The only non-zero component of the stress is therefore  $\sigma_{11}$ , which has a negative value. The resulting normal strain (= change in length) of the material along the  $X$  direction will be  $\varepsilon_{11} = s_{1111}\sigma_{11}$ , and will normally be negative indicating a compression. Values of the compliance tensor component  $s_{1111}$  are usually therefore positive. In addition, the directions along the perpendicular  $Y$  and  $Z$  axes may also change length;  $\varepsilon_{22} = s_{2211}\sigma_{11}$  and  $\varepsilon_{33} = s_{3311}\sigma_{11}$ . Note that terms such as  $s_{2211}$  are usually less than zero, so a normal compression along an axis results in expansion in the perpendicular directions. In addition to the normal strains, the compressive stress  $\sigma_{11}$  can also produce three shear strains, such as  $\varepsilon_{12} = s_{1211}\sigma_{11}$  (Fig. 3). The magnitude of each of the strains resulting from the applied stress is therefore dependent on the value of the corresponding component  $s_{ijkl}$ , with the sign of the component defining the direction, or sense, of the strain.

## 2.6. Stiffness tensor

The stiffness tensor, whose individual components are termed the “elastic moduli” of the material, is the inverse of the compliance tensor. The stiffness tensor, given the symbol  $c_{ijkl}$ , allows the stresses to be expressed as a function of the strains:  $\sigma_{ij} = c_{ijkl}\varepsilon_{kl}$ . The stiffness tensor also has 81 components. Note the confusing notation, that the stiffness tensor is represented by the letter  $c$ , while the compliance tensor is represented by the letter  $s$ .

## 2.7. Independent components

Although each elasticity tensor has 81 components, these are not all independent. First, because the stress and strain tensors each have only six independent components, the elasticity tensor itself can only have  $6 \times 6 = 36$  independent components. Further, the change in energy per unit volume of a body resulting from a set of strains  $\varepsilon_{ij}$  is given by the sum  $\frac{1}{2} \sum_{ijkl} c_{ijkl}\varepsilon_{ij}\varepsilon_{kl}$  over all of the strain components and tensor components. The energy for a given set of strains must be independent of the order in which the strains  $\varepsilon_{ij}$  and  $\varepsilon_{kl}$  are considered in the summation; this requires that the terms  $c_{ijkl}\varepsilon_{ij}\varepsilon_{kl}$  and  $c_{klij}\varepsilon_{kl}\varepsilon_{ij}$  must be equal. This can only be achieved if  $c_{klij} = c_{ijkl}$  (Nye, 1957, Chapter VIII) for all of the tensor components. Six of the 36 independent components of the tensor have equal subscripts (*e.g.*,  $c_{1111}$ ) and thus meet this criterion. The remaining  $(36-6)/2$  components must be 15 equal pairs, making a maximum of  $6 + 15 = 21$  independent components for the elastic modulus tensor. The same is true for the compliance tensor, which has  $s_{klij} = s_{ijkl}$ .

The elasticity tensors are material properties, and therefore must exhibit the symmetry of the material. The situation is entirely analogous to the optical properties of minerals that will be more familiar to those trained as mineralogists. The optical indicatrix, which defines the refractive indices and vibration directions for light passing through a crystal, is actually the representation surface of a second-rank tensor, the relative dielectric impermeability (Nye, 1957, chapter XIII). One recalls from optics that the crystal symmetry controls both the orientation of the indicatrix, and the relationship between the refractive indices for different directions in the crystal. For example, in tetragonal crystals, the refractive index is equal for all directions in the  $X$ – $Y$  plane, and different along the  $Z$  direction.

A crystal with triclinic symmetry has the full 21 independent components in its elastic tensors. In crystal systems of higher symmetry, some components are required by symmetry to be zero, and others are required to have specific numerical relationships to one another. For example, in cubic crystals,  $c_{1111} = c_{2222} = c_{3333}$ ,  $c_{1122} = c_{1133} = c_{2233}$ ,  $c_{1212} = c_{1313} = c_{2323}$ , and all other components are zero, yielding just three independent elastic tensor components. The number of independent components allowed for each Laue group symmetry is given in Table 1.

## 2.8. Matrix notation

The fact that the stress and strain tensors each only have six independent components allows the full tensor expressions for the stress–strain relationship to be reduced, for most calculations, to a matrix notation. In the matrix, or Voigt notation (Voigt, 1928), pairs of suffixes are reduced to a single suffix, which now runs from 1 to 6. Thus  $\sigma_{11}$  becomes  $\sigma_1$ ,  $\sigma_{22} \rightarrow \sigma_2$ , and  $\sigma_{33} \rightarrow \sigma_3$ . Terms with differing suffixes such as  $\sigma_{ij}$  take a single suffix equal to  $9-i-j$ , so that  $\sigma_{23} \rightarrow \sigma_4$ ,  $\sigma_{13} \rightarrow \sigma_5$ , and  $\sigma_{12} \rightarrow \sigma_6$ . The stress tensor is thus transformed to a vector with six components. A similar transformation can be applied to the components of the stiffness tensor so that, by taking the suffixes in pairs (e.g.,  $c_{1133} \rightarrow c_{13}$  and  $c_{1233} \rightarrow c_{63}$ ), the tensor is transformed in to a symmetric  $6 \times 6$  matrix. This enables the tensor equation  $\sigma_{ij} = c_{ijkl}\epsilon_{kl}$  to be replaced with the simpler matrix equation  $\sigma_m = c_{mn}\epsilon_n$ , in which the stresses can be

calculated by multiplying a vector of six strains by the matrix of coefficients of the stiffness tensor. However, in order to make this work numerically, the relationships between the strain tensor components and the elements of the strain matrix are:  $\epsilon_m = \epsilon_{ij}$  for  $i = j$  (i.e.,  $m = 1, 2$ , or  $3$ ), and  $\epsilon_m = 2\epsilon_{ij}$  for  $i \neq j$  (i.e.,  $m = 4, 5$ , or  $6$ ). The matrix equation that defines the strain resulting from an applied stress is  $\epsilon_i = s_{ij}\sigma_j$ . This requires the matrix elements to be defined as:

$$s_{mn} = s_{ijkl} \text{ when } m \text{ and } n \text{ are both } 1, 2, \text{ or } 3$$

$$s_{mn} = 2s_{ijkl} \text{ when either } m \text{ or } n \text{ are } 4, 5, \text{ or } 6$$

$$s_{mn} = 4s_{ijkl} \text{ when both } m \text{ and } n \text{ are } 4, 5, \text{ or } 6$$

Note that the matrices for both stiffness and compliance are symmetric;  $s_{mn} = s_{nm}$  and  $c_{mn} = c_{nm}$ . The matrix notation also has the advantage that the stiffness matrix is the inverse of the compliance matrix for all crystal systems, allowing for the simple conversion of moduli to compliances. However, there are a few cautions to be issued here. First, the conventions for converting compliance tensor components to matrix elements have differed in the past, and care must be taken to verify the convention used in the older literature (Nye, 1957, chapter VIII). Second, neither the individual matrix elements, nor the tensor components are generally the individual inverses of one another. That is,  $s_{mn} \neq 1/c_{mn}$  and  $s_{ijkl} \neq 1/c_{ijkl}$ , except for a very few specific individual cases in certain crystal systems. Third, the tensor components (not the matrix elements) must be used when performing transformations of axes, such as rotations. The matrix elements, and the matrices, do not transform correctly.

## 2.9. Cartesian reference systems

For ease of manipulation, both the elastic tensors and the stress and strain tensors, and their representations as matrices are always referred to a Cartesian set of reference axes. For orthorhombic, tetragonal and cubic crystal symmetries, the natural and common orientation of the Cartesian reference system is to have  $X$ ,  $Y$ , and  $Z$  parallel to the  $\mathbf{a}$ ,  $\mathbf{b}$ , and  $\mathbf{c}$  axes of the crystal. In these cases, the linear strains are then equal to the fractional change in the unit-cell parameters, for example  $\epsilon_1 = \Delta a/a$ . In the trigonal and hexagonal systems,  $Z$  is normally chosen to remain parallel to  $\mathbf{c}$ , and the  $X$  and  $Y$  axes then lie in the (001) plane. In the monoclinic and triclinic systems it is not possible to put all of the Cartesian axes parallel to crystal axes, and care must be taken to determine which of several conventions have been used before interpreting published values for the elastic tensor coefficients (Nye, 1957, Appendix B).

## 2.10. Hydrostatic pressure and bulk modulus

Hydrostatic pressure is a special state of stress in which there are no shear stresses, and in which the normal stresses

Table 1. The number of independent elastic tensor components for each Laue class.

Crystal system	Laue class	No. independent components
Cubic	m3, m3m	3
Hexagonal	6/m, 6/mmm	5
Tetragonal	4/mmm	6
Trigonal	3m	6
Tetragonal	4/m	7
Trigonal	–3	7
Orthorhombic	mmm	9
Monoclinic	2/m	13
Triclinic	–1	21

are equal in all directions, and equal to the pressure. If the pressure is denoted  $P$ , then the normal components of the stress tensor become  $\sigma_{ii} = -P$ , and the off-diagonal components are zero,  $\sigma_{ij} = 0$ . In the Voigt notation, this becomes  $\sigma_i = -P$  for  $i = 1, 2, \text{ or } 3$ , and  $\sigma_i = 0$  for  $i = 4, 5, \text{ or } 6$ . The elasticity equation defining the six strain components then becomes:  $\varepsilon_i = s_{i1}\sigma_1 + s_{i2}\sigma_2 + s_{i3}\sigma_3 = -P(s_{i1} + s_{i2} + s_{i3})$ . When a small increase  $\Delta P$  in pressure is applied to a crystal, then the change in stress is  $\sigma_{ii} = -\Delta P$ , and the resulting strains are  $\varepsilon_i = -\Delta P(s_{i1} + s_{i2} + s_{i3})$ . The volume strain is equal to the sum of the normal strains, so  $\Delta V/V = \varepsilon_1 + \varepsilon_2 + \varepsilon_3$ . Expanding the three equations for the linear strains leads to the expression for the volume compressibility of the crystal in terms of the compliance tensor components:

$$\beta_V = \frac{1}{V} \frac{\Delta V}{\Delta P} = s_{11} + s_{22} + s_{33} + 2(s_{12} + s_{23} + s_{13}) \quad (2)$$

The bulk modulus, defined as  $K = -V \partial P / \partial V$  is the inverse of the volume compressibility. These relationships between volume compressibility, bulk modulus and the compliance tensor apply for all crystal symmetries. In addition, under hydrostatic pressure, an analogous expression can be written for the linear compressibility of any direction within the crystal as  $\beta_l = s_{ijkl}l_i l_j$  in which the  $l_i$  are the three cosines of the angles between the direction of interest and the Cartesian reference axes  $X, Y, \text{ and } Z$  (Nye, 1957, chapter VIII).

### 2.11. Polycrystalline aggregates

When a polycrystalline aggregate is subject to hydrostatic pressure, all of the individual grains are subject to a stress that depends not only on the externally applied pressure, but that also depends on how the grains press on one another. For an aggregate of randomly oriented grains of a single material the value of the bulk modulus that expresses the variation of the volume with external pressure must lie between two limits called the Reuss and Voigt bounds. The Reuss bound represents an ideal situation in which the grains can slip past one another as pressure is increased, and every grain is therefore subject to a stress equal to the external pressure (Reuss, 1929). The Reuss bound of the bulk modulus is therefore equal to the value given in the preceding section for a single crystal under hydrostatic pressure. By contrast, if the grains are locked together, then each grain is subject to equal strain, and the bulk modulus is given by the Voigt bound (Voigt, 1928):

$$K_{\text{Voigt}} = \frac{c_{11} + c_{22} + c_{33} + 2(c_{12} + c_{23} + c_{13})}{9} \quad (3)$$

The Voigt and Reuss bounds for the bulk modulus of a material typically differ by a few percent, except for cubic crystals for which they are identical. In a similar way the average response of an isotropic aggregate of a single mineral to a shear stress is represented by the shear modulus,  $G$ ,

which can also be calculated from the components of the elastic tensors for each of the two bounding cases:

$$G_{\text{Reuss}} = \frac{15}{[4(s_{11} + s_{22} + s_{33}) - 4(s_{12} + s_{13} + s_{23}) + 3(s_{44} + s_{55} + s_{66})]}$$

$$G_{\text{Voigt}} = \frac{[(c_{11} + c_{22} + c_{33}) - (c_{12} + c_{13} + c_{23}) + 3(c_{44} + c_{55} + c_{66})]}{15} \quad (4)$$

The difference between the Voigt and Reuss bounds for the shear modulus increases with elastic anisotropy, even for cubic crystals (*e.g.*, Chung & Buessem, 1967), and can be very different in the neighbourhood of structural phase transitions (*e.g.*, Carpenter *et al.*, 2000).

### 2.12. Adiabatic and isothermal elastic response

When a material is compressed as a result of an applied stress, work is done on the system and, if the system is not allowed to dissipate this energy, it will heat up. In experimental methods such as static compression or mechanical analysis that employ relatively long time scales compared to atomic scale processes, this heat escapes to the environment and the experimental sample remains at constant temperature throughout the measurement. The elastic properties obtained from such experiments are termed *isothermal*, even if the sample is directly heated by the experimental probe to a constant temperature, and the isothermal bulk modulus is therefore defined as  $K_T = -V(\partial P / \partial V)_T$ . By contrast, experimental probes such as spectroscopy are fast relative to the time required to dissipate heat from a sample. As a consequence, the sample heats up as a result of the imposed stresses and the strains include the effect of the thermal expansion in addition to those arising from the stress alone. The values obtained for the elastic properties therefore differ from those measured isothermally. When the system remains completely thermally isolated and the strains are reversible (*i.e.*, elastic), the system is said to be *adiabatic*, and the entropy of the system remains constant. The adiabatic bulk modulus is thus  $K_S = -V(\partial P / \partial V)_S$ . The difference between the values of the individual components of the adiabatic  $s_{ijkl}^S$  and isothermal  $s_{ijkl}^T$  compliance tensors is given by (Nye, 1957):  $s_{ijkl}^S - s_{ijkl}^T = -\alpha_{ij}\alpha_{kl}T/C_p$ , in which  $\alpha_{ij}$  is the thermal expansion tensor,  $T$  is the temperature and  $C_p$  is the heat capacity at constant pressure. Because the thermal expansion tensor components are generally positive, the adiabatic compliances are normally smaller than the isothermal compliances. Differences between individual components are typically of the order of 0.1 % at room conditions. Conversely, the individual adiabatic moduli are typically larger than the isothermal moduli by the same ratio. Because the bulk modulus is equal to the sum of nine compliance tensor coefficients (Equations (2) and (3)), the correction term between isothermal and adiabatic bulk moduli is of the order of 1 %, except in the neighbourhood of a phase transition where it can be much larger. The

conversion between adiabatic and isothermal elasticity can also be expressed as a bulk average:  $K_S = K_T(1 + \alpha_V \gamma T)$ , in which  $\alpha_V$  is the volume thermal expansion coefficient, and  $\gamma$  is the thermal Gruneisen parameter (see Anderson, 1995). The adiabatic and isothermal values of the shear moduli are identical for crystals with higher than monoclinic symmetry under hydrostatic pressure (Wallace, 1972).

### 3. Stress–strain measurements

A conceptually simple way to determine the elastic tensor of a sample is to apply a known stress field and to measure the resulting strains. If a sufficient number of such measurements are made with different applied stress states, it is clearly possible to determine all of the values of the individual components of the compliance tensor. A historical review of the development of mechanical methods for applying known stresses to samples, and measuring the resultant strains, was given by Schreuer & Haussühl (2005), in which references to the older literature can be found.

#### 3.1. Direct mechanical methods

The stresses applied to a sample to determine its elasticity cannot be so large as to cause permanent plastic deformation or brittle failure. Because Earth materials are also relatively stiff, the resulting strains in a mechanical deformation experiment will also be small. As a consequence, direct mechanical measurements of the elasticity of minerals require samples of mm–cm size, in order for the strains to be measured with reasonable precision.

There are three common geometries for mechanical measurements of stress–strain curves. Tensile measurements, in which the change in length of a wire or a rod as a result of an applied load (stress) is measured, are common in metallurgy but less so for ceramic materials such as minerals because they tend to break under tension. In this geometry, the fractional change in length (the strain) is related to the applied stress as  $1/s'$ , where  $s'$  is the elastic compliance along the axis of the rod or wire. The quantity  $1/s'$  is known as “Young’s modulus”. Torsion experiments and three-point beam bending are used more often for mineral specimens and both can be applied to single crystal or polycrystalline specimens.

Three-point bending measurements require a sample in the form of a plate, typically 0.2–0.5 mm thick and 5 mm – 1 cm long that is supported on a pair of knife edges (Fig. 4). A known force is applied to the middle of the plate by a third knife edge. The resulting downward deflection of the plate,  $u_d$ , is related to the Young’s modulus,  $Y$ , of the direction parallel to the length of the plate by:

$$Y = \frac{l^3 F}{4t^3 w u_d} \quad (5)$$

in which  $l$  is the length of the plate between the outer knife edges,  $t$  its thickness, and  $w$  its width, and  $F$  is the applied

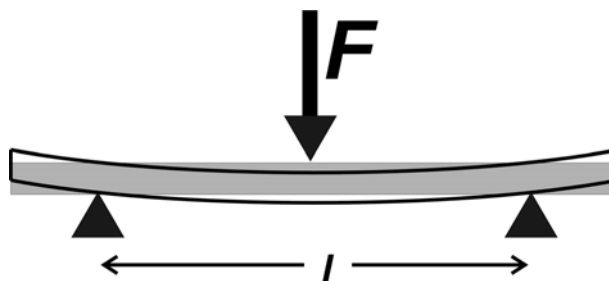


Fig. 4. The principles of a beam-bending experiment in which the deflection of a beam is measured as a function of the force  $F$  applied to the mid-point between two knife edges.

force. Because the method requires the measurement of strains by strain gauges, and large samples, it is restricted to measurements at room pressure. The temperature range is limited only by the properties of the sample, and that of the materials used to construct the instrument; measurements from very low temperatures of the order of 20 K up to 1000 °C have been performed (e.g., Schranz, 1997; Daraktchiev *et al.*, 2006).

The determination of the many components of the elastic tensor of a low-symmetry mineral by three-point bending measurements would require the cutting of a large number of single-crystal plates, which is often not practical and would certainly be time consuming. The technique is therefore more often used in a *dynamic* mode to explore the influence of defects such as domain and twin walls on the elastic properties of single crystals at seismic frequencies. In the dynamic mode the applied force from the central knife edge is modulated at frequencies between 0.01 and 100 Hz, and the displacement is measured as a function of time. In materials without defects, or ones in which they are immobile (e.g., due to low temperature) the deformation of the plate remains in phase with the applied force, and the material behaves elastically, and Young’s modulus is obtained. However, recent work (e.g., Harrison *et al.*, 2004a, b and c; Daraktchiev *et al.*, 2006), especially on perovskites, has shown that when defects such as twin walls become mobile at higher temperatures and low frequencies, the deformation lags behind the applied stress. The total deformation of the sample is then due to a combination of the elastic deformation of the ideal material plus the deformation induced by the defect motion. The technique is therefore very useful for studying these and similar processes on the 0.01–100 Hz time scale that are associated with structural phase transitions (Schranz, 1997). Such behaviour is generally termed “anelastic” and results in the absorption of energy, or attenuation (e.g., Harrison *et al.*, 2003). The geometry of the three-point bending apparatus readily allows it to be interfaced to other equipment so that the motion of the domains can be imaged by optical methods or X-ray diffraction (e.g., Harrison *et al.*, 2004b).

Torsion measurements have similar capabilities. They are performed on samples in the form of cylinders of typically 1 cm diameter and 3–5 cm in length; single

crystals could in principle be used, although the widest application has been to polycrystalline aggregates (*e.g.*, Webb *et al.*, 1999; Webb & Jackson, 2003) and to glasses and melts (*e.g.*, Webb & Dingwell, 1995; Webb, 2005). The principle is that a “twisting force” or torque is applied to one end of the sample, and the evolution of rotational strain is measured. The relationship between the stress and the strain then provides constraints on the shear moduli of the specimen. As for the three-point bending method described above, most experiments are performed in a dynamic mode called “forced oscillation” so that the time-dependence of various anelastic processes can be followed, in particular at seismic frequencies to provide insight into the propagation of seismic waves through rocks (*e.g.*, Aizawa *et al.*, 2008). For polycrystalline specimens an external pressure usually has to be applied to prevent deformation occurring by opening of the grain boundaries. Most experiments are therefore now performed in a “Paterson rig” (Jackson & Paterson, 1993) at modest pressures typically of the order of 200 MPa, and at temperatures up to 1300–1500 °C.

### 3.2. Resonance ultrasonic spectroscopy

Resonance ultrasonic spectroscopy (RUS) is, in a sense, a measurement technique that has similarities to direct mechanical methods, as well as exploiting the relationship between the elastic tensor and the properties of elastic waves in a solid. The technique, in all of its implementations, relies on the fact that solid objects have natural frequencies at which they vibrate when mechanically excited. A simple example would be a bell, which is machined so as to “ring” at a specific frequency when struck. The frequency is dependent upon the elasticity of the material, and the size and shape of the object. RUS exploits this property of solids to determine the elastic tensor of the material by measuring the natural “ringing” frequencies of an object, either a single crystal or a polycrystalline aggregate.

RUS can be applied to samples of a great range of sizes, from thin films to bridges, but for the measurement of mineral elasticity it is used on samples typically between 1 mm and 1 cm in size. The sample, either a fully compressed polycrystalline aggregate or a single crystal is machined in to a regular shape. It is held lightly between two piezoelectric transducers (Fig. 5). A sinusoidal signal is applied to one transducer, which drives the sample. The magnitudes of the resulting vibrations of the sample are monitored by the second transducer. The frequency of the input signal is then swept through a frequency range. At the resonant frequencies of the sample it rings like a bell, and the physical displacements of the second transducer are much greater than at other, non-resonant, frequencies. These resonant frequencies are then recorded. The elastic moduli cannot be determined directly from the resonant frequencies, even if the size and shape of the sample are accurately known. Instead, the resonance frequencies are calculated from the shape of the sample and an initial

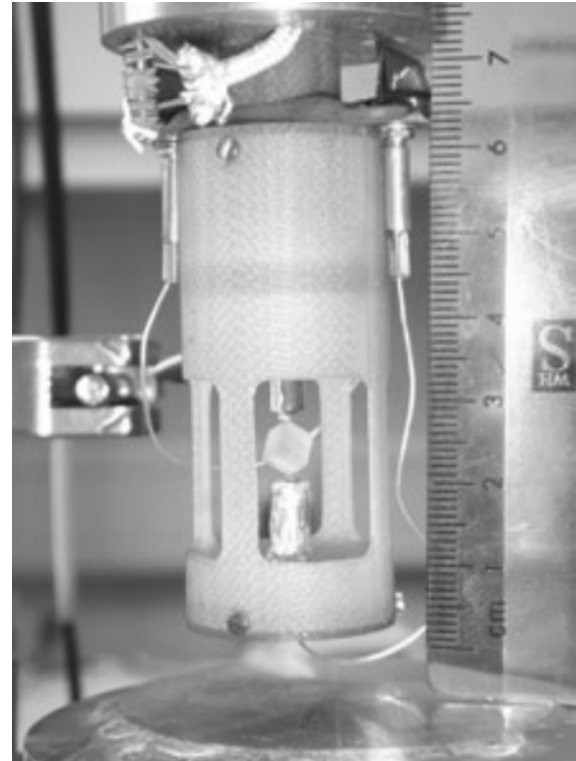


Fig. 5. The sample assembly for a resonance ultrasonic spectroscopy measurement showing the sample cube lightly held between the two buffer rods that transmit the ultrasonic excitations between the transducers and the cube. The entire assembly can be placed inside a cryostat for low-temperature measurements (McKnight *et al.*, 2007). Photograph courtesy of M.A. Carpenter (University of Cambridge).

estimate of the elastic moduli, and compared to the measured resonance frequencies. The values of the elastic moduli and the sample description are then adjusted in an iterative procedure until the sample spectrum is reproduced, at which point the elastic moduli have been determined. The principles of this analysis are clearly laid out by Migliori & Maynard (2005), and by Schreuer & Haussuhl (2005) for piezoelectric sample crystals.

For ease of data reduction, early measurements were performed on spheres, and the technique was then often termed the *resonant sphere technique* (*e.g.*, Oda *et al.*, 1992). Subsequent increases in computing power now allow the use of rectangular objects, and in general the resonances of a rectangular parallelepiped are normally measured in the version known as *RPR*. For variable-temperature measurements the sample is held between the ends of two buffer rods that link the sample to the transducers (Fig. 5) because the transducers must be kept at room temperature. The temperature range is then limited only by the properties of the furnace and buffer rods. Measurements up to 1500 °C (Isaak *et al.*, 1998a) have been reported. The technique is however limited to pressures of only a few bars, because the application of higher pressures leads to dampening of the resonances of the sample (Isaak *et al.*, 1998b).

The key to obtaining accurate values of elastic moduli with the RUS technique lies in the preparation and quality of the specimen. Polycrystalline samples should ideally be fully dense (although corrections for a few % porosity can be made) and free of cracks. Single crystal samples must be free of internal defects such as twin walls (although the dynamics of such defects can be investigated in a manner complementary to that of dynamical-mechanical methods). The surfaces of all samples must be polished flat and opposite faces should be parallel, but a good polish itself on the surface is not necessary. Once prepared, the density must be measured accurately as it scales the entire set of elastic moduli (see Migliori & Maynard, 2005).

While it was developed many years ago, the quantitative and routine application of RUS to the measurement of the elasticity of minerals has really developed within the last decade. The advent of digital signal generators and processing allows a wide range of frequencies to be scanned and the resonances measured in a matter of minutes, while modern PCs provide the computing power to rapidly perform the data reduction process, even for low-symmetry crystals (*e.g.*, Isaak & Ohno, 2003). The great advantage of the technique is that the entire elastic tensor is obtained from a single crystal sample in a single rapid measurement, in contrast to any other measurement technique. This means that the entire elastic tensor of a single-crystal sample can be readily measured over a wide temperature range, in a matter of hours. Such temperature scans provide a rapid method of determining the changes in elastic moduli associated with structural phase transitions (*e.g.*, Ohno *et al.*, 2006; Walsh *et al.*, 2008). Data reduction and analysis then often requires more time than the experimental measurements.

### 3.3. Measurements under hydrostatic pressure

Hydrostatic pressure is a special state of stress in which there are no shear stresses, and in which the normal stresses are equal in all directions, and equal to the pressure. Therefore, it can only be achieved in practice by immersing a sample in a pressure medium that has no shear strength, which means either a liquid or a gas. As for the direct mechanical methods described above, the determination of the compliance tensor from high-pressure experiments requires precise measurement of both the applied stress (*i.e.*, the pressure) and the resulting strains.

Hydrostatic pressure can be applied to a sample by a variety of high-pressure devices, including diamond-anvil cells, multi-anvil and piston-cylinder presses, and gas-pressure vessels. Each has its advantages and disadvantages, and each can accommodate very different sample sizes and can be used to explore very different pressure ranges with differing precision. For a general review of such devices, the reader can consult Keppler & Frost (2005). Once a hydrostatic stress has been applied to a sample in one of these pressure-generating devices, its change in length, or more generally in size and shape, has to be measured in order to determine the strain, and hence the elasticity of the sample. The practical difficulty is that

the properties of most physical devices, such as strain gauges, that are capable of measuring changes in the dimensions of the sample, also change with pressure. Therefore, successful measurements of the strain induced by hydrostatic pressure are limited to methodologies that probe the sample dimensions remotely.

### 3.4. High-pressure radiography

One such method was developed (Vaughan *et al.*, 2000; Kung *et al.*, 2002) for the multi-anvil press in conjunction with measurements by ultrasonic interferometry, described below, for which the length of the sample has to be known. These multi-anvil experiments are performed at a synchrotron beamline, at which an intense X-ray beam that is larger than the sample is shone through the sample assembly and the sample itself. The transmitted beam then illuminates a fluorescent screen and this light signal is then imaged with a CCD detector. The different components of the sample and surrounding assembly absorb the X-rays to differing extents, so that the sample casts a shadow in the image, whose change in length as pressure is increased can be used to determine the linear strain in the sample. The samples used are typically 1–3 mm in length, depending on the pressure range to be explored, and can be either single-crystal or polycrystalline powders. Pressures of 25 GPa can be achieved in some multi-anvil presses, although those on many synchrotron beamlines are limited to 10 or 15 GPa. One great advantage of the technique is that the experiments can be performed at high temperatures. Indeed, heating in these experiments is essential in order to anneal-out the non-hydrostatic stresses that develop in the solid pressure media surrounding the sample. While this method is a useful and necessary adjunct to determining elasticity by ultrasonic wave velocity measurements (see below), it is of relatively low precision compared to diffraction measurements. Further, for single-crystal measurements the methodology requires several sample loadings in order to determine the three-dimensional strain and is therefore not a practical alternative to diffraction.

### 3.5. High-pressure diffraction

High-pressure diffraction is the most widely used method by which the sample, held under high pressure, can be measured remotely in order to determine the pressure-induced strains. High-pressure diffraction can be performed on single crystals or powders, and with X-rays or neutrons. Details of the experimental methods and the differing requirements for samples are provided in detail by Hazen & Downs (2000). In brief, high-pressure X-ray diffraction measurements are usually performed using diamond-anvil cells to generate the pressure, so typical sample sizes range from  $0.1 \times 0.1 \times 0.03$  mm for single-crystal experiments in the 0–10 GPa pressure range to  $0.02 \times 0.02 \times 0.02$  mm for powder diffraction to megabar ( $\geq 100$  GPa) pressures. Single crystal diffraction is most often performed at room temperature, although a

few experiments have been performed at modest temperatures generated by external furnace elements (*e.g.*, Hackwell & Angel, 1995). X-ray powder diffraction in the DAC is routinely performed at simultaneous high temperatures and pressures, with heating provided in the 0–1500 °C range by external heaters (*e.g.*, Dubrovinskaia & Dubrovinsky, 2003) and by laser heating for higher temperatures (Fei & Wang, 2000). X-ray powder diffraction can also be performed with samples held in multi-anvil presses, but the restrictions on the angular access to the sample mean that angle-dispersive diffraction is severely limited so the method most often used is that of energy-dispersive diffraction. While such measurements are extremely useful for confirmation of phase identification, the lower resolution of energy-dispersive detectors limits their application for the precise measurement of lattice parameters. This, however, may change with the development of pixelated X-ray area detectors with energy discrimination.

Neutron diffraction requires larger sample volumes and is thus restricted to lower pressures than can be achieved with X-ray diffraction. Both powders and single crystals have been studied at pressure with Paris-Edinburgh type cells, which typically require several mm<sup>3</sup> of sample and can now reach up to 20 GPa, although maximum pressures in the 5–10 GPa range are more common. Panoramic anvil cells, essentially variants on diamond-anvil cells with much larger anvils and operated so that the incident and diffracted X-ray beams pass through the cell approximately perpendicular to the load axis, have been developed for high-pressure single-crystal diffraction with neutrons. Single crystal sizes are typically 0.5 mm on an edge, although the advent of neutron sources of increased intensity, such as the Spallation Neutron Source (SNS) in the USA, means that this may gradually decrease to 0.1 mm on edge (Ross & Hoffmann, 2006). However, the demand for time on the limited number of beam lines with the facilities for such experiments means that it is not practical to do neutron diffraction measurements merely to measure lattice parameters at high pressures, especially as more precise results can be obtained by X-ray diffraction.

High-pressure diffraction experiments provide direct measurements of the unit-cell parameters and volume of the unit cell of the sample. Changes in the unit-cell parameters associated with a change in pressure can then be transformed into a set of strains,  $\varepsilon_i$ , from which values of the elastic compliances can be determined. However, the elasticity equations introduced in the previous section explicitly assume that the strain induced in a material is proportional to the applied stress. While this is true for small strains, the strains induced by high-pressure experiments are not small. For example, linear strains in minerals compressed to 10 GPa will typically be between 1 and 7 %, and volume strains between 3 and 20 %. After these strains the atoms are significantly closer together at higher pressures, and the repulsive forces between them are significantly stronger, than at ambient pressure. The material is therefore stiffer at higher pressures (and the compliances decrease in magnitude). Two modifications to the elasticity equations are required to accommodate this

behaviour. They are most easily illustrated for the case of the volume variation with pressure. First, the infinitesimal volume strain  $\Delta V/V$  is replaced by an appropriate definition of *finite* strain. Second, a form of the variation of the bulk modulus with pressure (or strain) is defined. There are various choices for both definitions; each combination is termed an ‘‘Equation of State’’ (*e.g.*, Anderson, 1995; Angel, 2000). There is no thermodynamically correct choice for an Equation of State, but it is found that the Birch-Murnaghan EoS, based upon the finite Eulerian definition of strain provides the best fit to experimental  $P$ - $V$  data, and the best match to independent measurements of the compliance tensors (*e.g.*, Birch, 1947; Anderson, 1995; Angel, 2000). The Equation of State is fit to the  $P$ - $V$  data to obtain values of the isothermal bulk modulus and its pressure derivatives at a reference pressure ( $K_{0T}$ ,  $K'_{0T} = \left(\frac{dK}{dP}\right)_{0T}$ ), from which the value of the bulk modulus at any pressure can be calculated (Angel, 2000). The precision of the value of the bulk modulus depends on several factors. The precision of  $K_0$  increases with the precision and number of data points and the pressure range over which the data were collected, but decreases as the value of the bulk modulus of the material itself increases (Angel, 2000). Single-crystal diffraction experiments on typical minerals ( $K_0 \sim 100$  GPa) to a maximum pressure of 10 GPa with pressure determined from internal diffraction standards typically yield formal uncertainties in  $K_0$  of around 0.5 GPa or better, and carefully-collected and analysed powder diffraction measurements can approach similar levels of precision.

In addition to the variation of unit-cell volume, the variation in the cell parameters with pressure can be used to define a strain tensor, each component of which provides the sum of three compliance tensor components ( $s_{i1} + s_{i2} + s_{i3}$ ) =  $-\varepsilon_i/P$ . Note that this means that measurements of the changes of unit-cell parameters induced by hydrostatic pressure can never yield individual values of the compliances of the crystal, only sums of compliances. Following the example of volume, it is appropriate to use the Eulerian finite strain tensor because of the relatively large strains involved. There are then two approaches that can be used to extract the variation in a compliance sum ( $s_{i1} + s_{i2} + s_{i3}$ ) with pressure. For crystals of orthorhombic symmetry or higher, the unit-cell angles do not change with pressure, the strains  $\varepsilon_4$ ,  $\varepsilon_5$ , and  $\varepsilon_6$  are thus zero, and only the cell edges change in length. It has been found (Angel, 2000) that, in these cases, reliable values of the compliance sums can be obtained by cubing each cell parameter in turn and fitting each with a Birch-Murnaghan EoS. The resulting axial compressibilities fully describe the evolution of the unit-cell with pressure. But for monoclinic crystals one unit-cell angle may change, and in triclinic crystals all three unit-cell angles may change. The full description of the change in unit-cell shape in these cases must therefore include the full definition of the strain tensor resulting from compression; for monoclinic there are four equations ( $s_{i1} + s_{i2} + s_{i3}$ ) =  $-\varepsilon_i/P$ , with  $i = 1, 2, 3$ , and 5 (for

**b**-axis unique), and all six equations for triclinic crystals. One approach is to collect the data at reasonably small pressure intervals (*e.g.*, 0.3–0.5 GPa), and calculate from the unit-cell parameters the Eulerian finite strain induced from one pressure datum to the next. When the resulting compliance sums are plotted against the mean pressure of the pairs of data points, the variation in compliance sums matches that determined by direct fitting of the cell parameters, and yields estimates of the room pressure compliance sums that agree with independent measurements (*e.g.*, Brown *et al.*, 2006; Johnson, 2007).

### 3.6. Diffraction under non-hydrostatic stress

It can be seen that under hydrostatic conditions the measurement of the variation of the unit-cell parameters with pressure only yields approximately one-third of the equations necessary for determining the full elastic tensor of a crystal (*i.e.*, one equation for three tensor components in cubic symmetry, or six equations for 21 tensor components in triclinic symmetry). In principle, the application of several different non-hydrostatic stress states to a sample in a diffraction experiment could provide additional constraints to allow the determination of all the tensor components. For example, in a DAC powder diffraction experiment Singh *et al.* (1998) showed that the shift in *d*-spacings of diffraction lines is consistent with the grains being under a uniform non-hydrostatic stress in which the axial stress parallel to the diamond-cell axis is higher than the radial stress. The *d*-spacing of a reflection then depends on the orientation of the plane normal to the stress field and the elastic constants (Singh *et al.*, 1998; Dubrovinsky & Dubrovinskaia, 2004). The theory (Uchida *et al.*, 1996; Singh *et al.*, 1998) allows the determination of the elastic moduli (at least of cubic minerals), without independent measurements of the stress fields. Some results are available for cubic and hexagonal minerals (Speziale *et al.*, 2006 and references therein), but there are strong doubts about the reliability of the method, due to the very high stress levels and the subtle effects of plastic deformation on the interpretation of the experimental results (Weidner *et al.*, 2004).

When single crystals are subject to non-hydrostatic stress fields the diffraction maxima exhibit both shifts in position and line broadening, indicating that the sample is under both non-uniform and non-hydrostatic stress. Nonetheless, it can be shown that the deviation in the average cell parameters from their values under hydrostatic conditions can be explained in terms of the orientation of the crystal with respect to the stress field, and the elastic tensor of the crystal (Zhao & Angel, *in prep.*). However, the values of the elastic tensor components cannot be extracted from such measurements without independent measurement of the applied stress field. It should also be remembered that it is not only the behaviour of the sample that is affected by non-hydrostatic stresses, but pressure sensors such as ruby also yield incorrect apparent pressures under such conditions (Chai & Brown, 1996). The combination of unknown stress state combined with

difficulties in defining the pressure make diffraction under non-hydrostatic conditions a poor method of determining the elastic tensors of crystalline materials.

### 3.7. Computational methods

Modern computational methods are based upon the concept of accurately simulating the atomic arrangement, thermodynamic properties and often dynamics, of a structure. Computational methods fall in to two general classes (*e.g.*, Stixrude *et al.*, 1998). Those based upon *ab initio* or *first-principles* methods aim to calculate the interactions between atomic cores and the electrons. Methods based upon *interatomic potentials* model the forces between atoms by assigning a specific model to the various bonded and non-bonded interactions. Both approaches then seek to find the stable configuration of the atoms by adjusting the components of the structure so as to minimize its energy. Simulations can be performed at zero temperature, and a number of methods exist to simulate the effects of temperature (*e.g.*, Jung & Oganov, 2005). In all cases, once the equilibrium lowest-energy configuration of the structure has been found, the elastic tensor can be determined in one of three ways. Some simulation packages provide the tensor components directly from the calculation of the second derivative of the free energy with respect to deformations or strain (*e.g.*, Wentzcovitch *et al.*, 1993). Or, in a conceptually equivalent method, the user can introduce specific strains in subsequent calculations, minimize the energy of each strained structure, and thus extract the values of the tensor components. A third approach is to perform a series of simulations at various pressures and extract the compressional moduli from the resulting unit-cell parameters in the same way as described above for diffraction experiments.

The accuracy of the calculated elastic moduli depends on the calculation method, and on the effort expended to ensure that a true equilibrium configuration has been obtained at both the pre-stressed state and the stressed state. For static calculations (which means a model calculation at 0 K without including lattice-vibrational zero-point motion), the *ab initio Local Density Approximation (LDA)* method tends to underestimate the equilibrium volume, especially of more open framework structures, and thus overestimates the elastic moduli, while the *ab initio Generalized Gradient Approximation (GGA)* overestimates volumes and underestimates moduli (Karki *et al.*, 2001). However, at finite temperatures, when the lattice vibrational effects are included in the free energy calculations through a quasi-harmonic approximation, the LDA method provides elastic constants and Equation of State parameters that are very close to experimental values (*e.g.*, Wentzcovitch *et al.*, 2004; Yu & Wentzcovitch, 2006). In contrast, the results from GGA calculations at finite temperatures are in poorer agreement than those at 0 K. The accuracy of calculations based on interatomic potentials depends mostly upon the care taken in determining the potentials. They often provide values for the elastic properties that are as accurate as those from *ab initio* calculations, especially for the bulk and shear moduli.

#### 4. Wave velocity measurements

The velocities of acoustic waves in solids are intimately related to the elastic properties of the material. In this section we describe the principles of several experimental techniques that determine the elasticity of materials by determining the speeds of acoustic waves travelling through the sample. The propagation of acoustic waves involves the small displacement of adjacent particles (*e.g.*, atoms) within the material. Because the atoms are connected together, the displacement of one atom leads to the displacement of adjacent atoms, and the displacement is thus propagated through the material. Acoustic waves can be divided in to two types based on the relative orientation of the particle displacement and the direction of propagation of the wave (Fig. 6). Compressional, longitudinal, or *p*-waves involve particle motion along the direction of propagation, thus giving rise to a pattern of compression and rarefaction along the propagation direction. In contrast, when the particle motion is perpendicular to the propagation direction the waves are termed transverse or shear or *s*-waves. It should be clear from this description that the restoring forces on the particles that arise from their small displacements must be determined by the elastic properties of the material. The general relation is:

$$\rho \frac{\partial^2 u_i}{\partial t^2} = c_{ijkl} \frac{\partial^2 u_k}{\partial x_j \partial x_l}, \quad (6)$$

where  $\rho$  is density of the material, and  $u$  is the displacement. The experiments that determine elasticity by measuring wave velocities generate plane waves. By substitution of plane wave solutions in to Equation (6) a set of linear equations is obtained which relates the particle displacement (or polarization) to the direction of the wave, represented by its direction cosines  $l_{i,j}$ , and its velocity  $v$ :

$$(c_{ijkl} l_j l_l - \rho v^2 \delta_{ik}) U_k = 0 \quad (7)$$

The displacements are represented by the three components  $U_k$ , and  $\delta_{ik}$  is the Kronecker delta ( $\delta_{ij} = 1$  for  $i = j$ ,  $\delta_{ij} = 0$

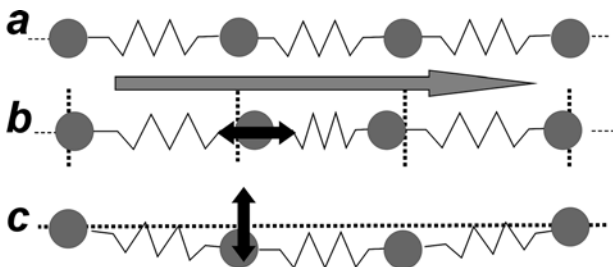


Fig. 6. Particle motion in waves. The direction of wave propagation is to the right (large arrow) and the particle motion is indicated by the smaller double arrows. (a) Undisturbed particles. (b) In a compressional wave the particle motion is along the propagation direction. (c) In a shear or transverse wave the particle motion is perpendicular to the propagation direction.

for  $i \neq j$ ). The determination of elastic moduli then requires measurement of wave speeds, propagation directions and whether the waves are shear or compressional (to determine  $U_k$ ). In addition, it should be noted that the density  $\rho$  of the sample scales the relationship between velocities and the elastic moduli. Therefore accurate determination of the density is an essential adjunct to all measurements of elasticity from wave speeds.

In elastically isotropic solids such as polycrystalline aggregates or glasses, the compressional and shear wave velocities are independent of the wave propagation direction, and they are related to the adiabatic bulk and shear moduli as:

$$V_p = \left[ \frac{(K_S + 4/3G)}{\rho} \right]^{1/2}, \quad (8)$$

$$V_s = \left( \frac{G}{\rho} \right)^{1/2}$$

In fluids the shear strength and hence the shear modulus,  $G$ , are zero so shear waves cannot be propagated. The compressional velocity is then related to adiabatic bulk modulus as:

$$V_p = \left( \frac{K_S}{\rho} \right)^{1/2}. \quad (9)$$

##### 4.1. Ultrasonic travel time measurements

The aim of ultrasonic experiments is to measure the travel time of high-frequency acoustic waves through the sample. Sample sizes range from 0.1 mm to a few cm, so high frequencies, in the MHz or GHz range, are required to ensure that the wavelength of the acoustic waves is significantly shorter than the sample thickness. The wave velocity is then determined from the travel time and the length of the sample. Since wave velocities in minerals are of the order of  $\text{km s}^{-1}$ , the experimental challenge is to measure travel times of  $10^{-5}$ – $10^{-8}$  s to sufficient precision.

Ultrasonic waves are generated by piezoelectric crystals (transducers), such as ZnO, LiNbO<sub>3</sub> or SiO<sub>2</sub>, whose dimensions change when an electrical voltage is applied to them. In nearly all ultrasonic experiments the sample is not fixed directly on to the transducer, but a buffer rod is used between the transducer and the sample. The application of an alternating voltage to the transducer results in a vibration of the transducer with the same frequency as the input electrical signal. If the transducer has tight mechanical contact to the buffer rod and the buffer rod has tight contact to the sample, sound waves (= stress waves) will travel from the transducer through the buffer rod and the sample. A simple way to measure wave velocities is then to fix buffer rods and transducers on two opposite sites of the sample. One transducer

generates a pulse of sound waves and the second one detects them. The time delay between the generation on one side and the detection of the stress waves on the other side of the sample is the travel time, and is determined electronically (e.g., Kern & Tubia, 1993). However, this method works only for samples as large as several millimetres, because the uncertainty in travel-time measurement would be too large for smaller samples. Moreover, it is very difficult to apply this method in multi-anvil apparatus or in diamond anvil cells.

## 4.2. Ultrasonic interferometry

When acoustic waves pass across a boundary from one material to another with different elastic properties, some of the energy is reflected back as a second acoustic wave. Interferometry uses the interference between waves reflected from the two ends of the sample to determine travel times, and hence velocities. A signal generator is used to generate two sinusoidal pulses of voltage that are applied to the transducer to generate two travelling pulses of sound waves in the buffer rod (Fig. 7). A portion of the first pulse of the sound waves is reflected at the front of the sample at the boundary with the buffer rod, while another portion of the same pulse travels on through the sample and is reflected from its back face. The second pulse is sent after a time delay  $\Delta t$  chosen such that the buffer rod echo from the second pulse overlaps with the echo of the first burst from the back of the sample (Fig. 7). The two echo bursts with time delay  $\Delta t$  overlap with each other and travel back to the transducer which converts the combined burst back to an electrical signal. The first burst has travelled an extra distance of twice the sample thickness. Therefore constructive interference between the two bursts occurs when the frequency of the waves is such that twice the sample thickness is an exact integer multiple of the wavelength,  $\lambda$ . Since wavelength changes with frequency, sweeping the frequency gives rise to a sinusoidal interference pattern of maxima and minima (Fig. 8a) in the interfered returned signals. Destructive interference occurs when the twice the thickness of the sample is exactly equal to an odd number of half-wavelengths. The travel time of the sound waves can now be calculated from this interference pattern via the equation

$$t = \frac{m}{f_m} \quad (10)$$

where  $t$  is round trip travel time, the value  $m$  is either integer (for maxima) or an odd multiple of half an integer (for minima) and  $f_m$  is the frequency at which the maxima and minima occur (Spetzler *et al.*, 1993, 1996). To calculate  $t$ , the frequency  $f_m$  needs to be determined. To obtain  $f_m$ , a second order polynomial curve is fitted separately to every maxima and minima. The vertex of each curve is taken as the frequency  $f_{\max}$  or  $f_{\min}$  (Fig. 8a), and the travel time  $t = m/f_m$  is then plotted versus frequency (Fig. 8b), to obtain an average round-trip travel time  $t$ . The precision of travel time determination at ambient conditions is about  $10^{-5}$  (Spetzler *et al.*, 1993); the precision of velocities then depends on the measurement of the sample thickness.

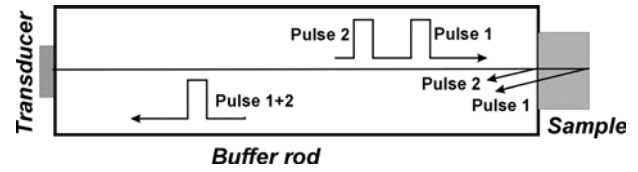


Fig. 7. The principles of ultrasonic interferometry with a buffer rod. Two coherent pulses of sound waves are sent along the buffer rod towards the sample with a time delay so that the reflection of the first wave pulse from the far end of the sample overlaps and interferes with the reflection of the second wave pulse from near end of the sample.

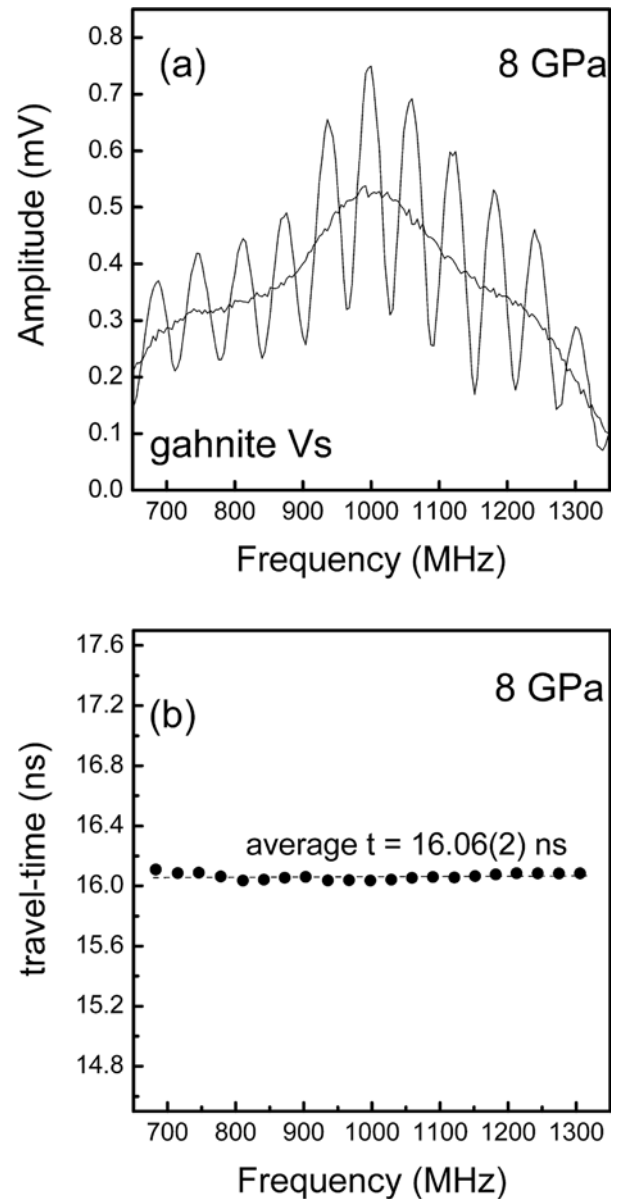


Fig. 8. (a) Interference pattern from a DAC high pressure experiment on gahnite at 8 GPa. The solid line in the spectrum is the frequency response of the system without sample. (b) The  $V_S$  – travel time data extracted from the spectrum. Each dot corresponds to a travel time from the respective maximum or minimum.

Ultrasonic interferometry can be combined with piston-cylinder or multi-anvil presses to measure the elastic properties of minerals at P – T conditions in the Earth’s crust and mantle. Though the internal arrangements of the various presses differ, the principles of ultrasonic interferometry experiments are the same. The acoustic signals are generated by a transducer, whose resonance frequency is at about 30–50 MHz (the samples in these high pressures devices are typically as long as 1–2 mm, the frequencies of the sound waves are in the MHz range). In the case of a multi-anvil apparatus the transducers for the *p*- and *s*-waves are glued on to the free outer surface of one of the tungsten carbide anvils, so that the transducers do not experience any pressure. The sound waves generated by the transducers travel through the anvil to the sample, and return by the same path. The anvil thus acts as a buffer rod, and the data acquisition and processing methods are as described above.

Ultrasonic travel time measurements in multi-anvil apparatus are usually determined with an accuracy of better than 0.3 % (Mueller *et al.*, 2005b). The uncertainty in the wave velocities is then dominated by the uncertainty of the sample length determination. Cook’s method allows the calculation of the sample length at pressure from a sequence of measurements of the travel times of the sound waves through the sample at high P – T conditions (Cook, 1957; Kung *et al.*, 2001; Li, 2003). For experiments in multi-anvil apparatus at synchrotron (X-ray) sources, the whole press can be scanned across the beam and the diffraction pattern monitored (Mueller *et al.*, 2003). The distance the press is moved between the first and the last appearance of the sample diffraction pattern is the sample length. This scan takes about half an hour to determine the sample length, so X-ray radiography, discussed in a previous section, is often used as a faster and more accurate method (*e.g.*, Kung *et al.*, 2002; Gwanmesia *et al.*, 2006; Li *et al.*, 2006). The change in sample length can also be obtained from measurement of the unit-cell volume by *in situ* diffraction, or simply estimated from a previously known equation of state (*e.g.*, Jackson & Niesler, 1982; Chen *et al.*, 1998; Li *et al.*, 1998).

To decrease the uncertainties in travel time measurements, one has to detect as many maxima and minima of the interference pattern (Fig. 8) as possible. This requires measurements over a broad frequency range, which is time consuming. To speed up the experiments – which is for example of great importance for rheology or kinetic experiments at high *P* and high *T* conditions – the transfer function method can be used (Li *et al.*, 2002; Mueller *et al.*, 2005a). This records the system response to all frequencies within the pass band at one time rather than sweeping through the frequencies as in “conventional” methods. Recording the transfer function thus takes a few seconds compared to 20 min to 1 h for a frequency sweep.

Ultrasonic interferometry has also been interfaced with diamond-anvil pressure cells. The additional challenges arise from the small size of the sample, typically 30–50  $\mu\text{m}$  thick. This requires shorter wavelengths to be used, no more than 10  $\mu\text{m}$ , which in turn means the frequencies are

in the GHz regime, rather than the 30 MHz typically used in multi-anvil experiments. GHz *p*-wave transducers have to be specifically fabricated (Spetzler *et al.*, 1993), but all efforts to produce GHz – shear wave transducers have failed. Instead, *p*-wave transducers are used, and the *p*-waves are converted to *s*-waves by reflection from the surface of an yttrium aluminium garnet prism, which also acts as the buffer rod (Jacobsen *et al.*, 2002). The travel time uncertainty of GHz-experiments at zero pressure is about  $10^{-5}$ , and at high pressure in a DAC about  $10^{-3}$ . Because it is impossible to measure the length of the sample under pressure in a DAC “mechanically”, the sample length has been determined by independent measurements of unit-cell parameters or by utilizing the known EoS of the sample (*e.g.*, Reichmann *et al.*, 1998; Kantor *et al.*, 2004).

Ultrasonic interferometry has the advantage that it can be applied to glasses, melts, polycrystalline materials and single crystals, and is readily interfaced to high-temperature furnaces (*e.g.*, Nasch *et al.*, 1994; Webb & Dingwell, 1994; Webb & Courtial, 1996) and high-pressure devices. Except for single-crystal samples, two measurements, of *s*- and *p*-wave velocities on a single sample suffice to entirely characterize the bulk elasticity in terms of the bulk and shear moduli *K* and *G*. Thus the method is very suitable for following the evolution of these parameters as a function of pressure and temperature (*e.g.*, Jackson & Niesler, 1982; Gwanmesia *et al.*, 2006) and for the determination of cross-derivatives of the elastic moduli ( $\partial^2 c_{ij} / \partial P \partial T$ ) (Chen *et al.*, 1998). However, a complete determination of the elastic tensor of low-symmetry materials requires many measurements of travel times in many different directions of a single-crystal sample. This has mainly restricted the use of ultrasonic interferometry to high-symmetry single crystals (*e.g.*, Yoneda, 1990; Jacobsen *et al.*, 2004; Kantor *et al.*, 2004; Reichmann & Jacobsen, 2006) although orthorhombic single-crystal olivine has been measured to 3 GPa (Webb, 1989).

### 4.3. Impulsively stimulated laser scattering (ISLS)

The term *ISLS* covers several different measurement techniques that differ in detail, but that use essentially the same physical principles. A pair of laser pulses (with wavelengths in the near infrared range) is arranged so that they intersect and interfere within the sample (or on its surface). This produces, by optical absorption and thermal expansion, a pattern of heated areas and a pattern of variations of the dielectric constant (*e.g.*, Brown *et al.*, 1989; Zaug *et al.*, 1994; Crowhurst *et al.*, 2005). In addition, a set of propagating acoustic waves is generated in the sample. Both the static thermal pattern and the propagating acoustic waves behave as diffraction gratings for light from a third laser, known as the probe, which is then Bragg diffracted. In principle, the time dependence of the intensity of this diffracted beam as the thermal grating decays, together with knowledge of the experimental geometry, allows the acoustic velocities of the waves to be

determined (Zaug *et al.*, 1992; Crowhurst *et al.*, 2005). With sufficient data coverage, the elastic moduli can then be determined from the wave velocities by application of Equation (7).

In transparent or almost transparent materials the acoustic waves produced by the exciting pulses are mainly body waves, inside the sample, whereas for opaque materials the stimulated acoustic waves are mainly surface waves. In the case of samples immersed in a medium (such as in diamond-anvil cells) interfacial waves are also stimulated. The surface or pseudo-surface waves are not only sensitive to the surface properties of the sample. In fact, the penetration depth of the surface acoustic waves is of the same magnitude as the wavelength, which is of the order of few microns, so that these waves provide information about the elasticity of the bulk of the material (Crowhurst & Zaug, 2004). The analysis of surface wave data is complex, but the theory is well-developed and can be applied to crystals of any symmetry and to different experimental geometries (Every *et al.*, 1997; Every & Briggs, 1998; Maznev *et al.*, 1999; Crowhurst & Zaug, 2004). In particular, it has been demonstrated that surface wave data can be collected from non-absorbing transparent minerals at room pressures by simply polishing oriented surfaces and then coating them with a thin metal layer. With well-chosen orientations, the full elastic tensor of even triclinic minerals can be determined from measurements on five or six polished plates relatively rapidly (*e.g.*, Brown *et al.*, 2006). It should be noted that surface wave measurements constrain the differences between moduli significantly better than the values for some individual moduli. The technique is thus complementary to high-pressure diffraction that provides constraints on the sums of moduli. Data from the two methods can thus be combined to yield more precise values for all of the components of the elastic tensor (Brown *et al.*, 2006).

One critical limitation on the precision of ISLS surface-wave measurements is the orientation of the sample with respect to the exciting laser beams. This only becomes an issue in the diamond-anvil cell, in which case it is important that all the interfaces between the elements of the sample assembly are flat and parallel. The reproducibility of ISLS measurements is better than 0.1 % on the acoustic velocity at high pressures in the diamond-anvil cell. Misalignments and defective surface quality can degrade the reproducibility to values of around 0.5 %.

The great advantage of ISLS is that it can be used to measure the elasticity of opaque samples in the diamond-anvil cell (Crowhurst *et al.*, 2001). ISLS has been recently performed on (Mg<sub>0.94</sub>Fe<sub>0.06</sub>)O compressed up to 60 GPa to investigate the effect of spin transition of Fe in the second most abundant mineral of the lower mantle (Crowhurst *et al.*, 2008). By combining surface (interfacial) acoustic velocities measured by ISLS and independent density measurements at high pressures Crowhurst *et al.* (2005) determined bulk and shear moduli of polycrystalline Co and Fe up to 120 GPa, and similar measurements on single crystal Co to determine the full elastic tensor have been performed to 10 GPa (Crowhurst *et al.*, 2006). Simultaneous

high-pressure and high-temperature ISLS has been performed on molecular compounds such as H<sub>2</sub>O up to 400 °C and 5.5 GPa (Abramson & Brown, 2004).

#### 4.4. Phonons and dispersion

In a crystal, atoms vibrate around their equilibrium positions. The vibrations of atoms are not independent of one another, but are coupled because of the bonding between the atoms. The collective motions of the atoms correspond to waves within the crystal. The full description of the motions of the atoms in a crystal is the field of *lattice dynamics*, to which a good introduction can be found in Dove (2003), but a brief description is offered here. If there are  $N$  atoms in the primitive unit-cell of a crystal, then there are  $3N$  waves for any given combination of wave propagation direction and wavelength  $\lambda$  (corresponding to a single *wave vector*). Each of these  $3N$  vibrational modes corresponds to a different pattern of relative displacements of adjacent atoms, and thus each has a different natural vibrational frequency that is dependent upon the forces between the atoms. Figure 6 illustrates the basic phenomena for a 1-D string of atoms. The frequency of any given mode also changes with wavelength, even for a single direction, because the magnitudes of the relative displacements of adjacent atoms will change as the wavelength changes. Plots of the frequency variation of the modes with wave vector  $\mathbf{k}$ , with modulus  $k = 2\pi/\lambda$ , are dispersion curves (*e.g.*, Fig. 9). As for any other microscopic property, the energy of each of these vibrational modes is quantized, and this leads to an equivalent description of lattice vibrations in terms of quanta of vibrational energy called phonons. Phonons are the ‘‘particle’’ equivalent of the lattice vibrations in the same way that photons are the particle equivalent of light and other electromagnetic radiation.

For any propagation direction in the crystal just three of the collective motions have all of the atoms inside the unit cell move in-phase with one another (at least for long wavelengths or short wave vectors). These special modes are termed acoustic modes. Their frequency goes to zero at long wavelengths (which is equivalent to wave vectors of almost zero in the dispersion diagram). It is these modes that are probed by Brillouin spectroscopy close to the origin or *zone centre* (*i.e.*, at very long wavelengths) and by inelastic X-ray and neutron scattering techniques at shorter wavelengths (Fig. 9). The remaining  $3N - 3$  modes involve relative motions of the atoms inside the unit cell that are out-of-phase with one another. They are called optic modes, and do not play a role in elasticity. They are probed by various optical spectroscopies and also by inelastic scattering methods.

An integration over all of the modes at all wave vectors represents a summation of all of the vibrational modes of the atoms within the crystal, and is known as the *phonon density of states* (PDOS or DOS). It is an important quantity to describe the low-energy collective states of solids and is used to calculate thermodynamic properties related to lattice vibrations and specifically elastic properties.

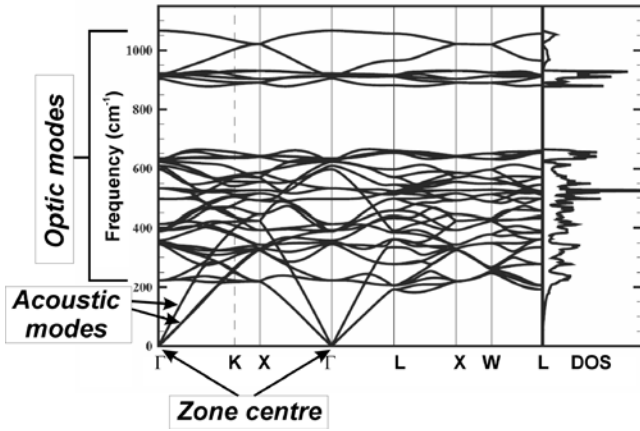


Fig. 9. Calculated dispersion curves for a spinel (Y. Yu, pers. comm.) showing how the frequency of each vibrational mode changes with the wave vector (direction and wavelength). Different sectors of the unit cell are shown, divided by the thin vertical lines. Special points in the Brillouin zone are labelled by specific letters; the “ $\Gamma$  point” is the zone centre, and the other points are on the boundary of the Brillouin zone. Brillouin spectroscopy measures the acoustic modes very close to the zone centre; other modes can be measured by inelastic scattering techniques, and the optic modes at the zone centre by infra-red and Raman spectroscopy. The Density of States (DOS) shown on the right is an integration over all of the modes in all directions, and can be measured by Nuclear Resonant Inelastic X-ray scattering.

It can be obtained, at least in part, by inelastic scattering techniques.

#### 4.5. Brillouin scattering

The theory of the Brillouin effect in solids and fluids differs in the details (see a comprehensive review in Cummins & Schoen, 1972). However, the experimental approach is the same for both fluids and solids, and this description applies to crystals. The acoustic modes in a crystal are identical at long wavelengths to acoustic elastic waves. The velocities of these waves are therefore related to the relevant elastic moduli and the density as  $v^2 = c/\rho$ , and in detail by Equation (7).

In a Brillouin scattering measurement the wave velocity is measured by shining an intense monochromatic laser light on the sample. A small fraction of the laser light interacts with the collective acoustic vibrations. In some interactions the incoming laser light excites the vibration, meaning that energy is transferred from the light to the vibration, so that the corresponding light scattered by the sample has a lower energy than the incident light. This is known as Stokes scattering. It is also possible for energy to be transferred from the acoustic mode to the incident light, resulting in an increase in frequency of the scattered light in anti-Stokes scattering. A particle representation of this process, in terms of exchange of a quantum of energy between the incident radiation and the phonon representing the lattice vibration, is given in Fig. 10. The frequency of the scattered light is then measured by a high-resolution

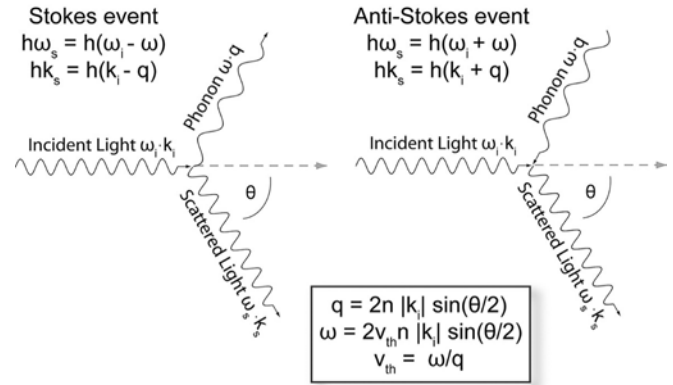


Fig. 10. The two types of inelastic interaction between incident radiation and the vibrational modes in a crystal, as represented by phonons. In each case, a quantum of energy  $h\omega$  is exchanged. In a Stokes event the energy is transferred to the phonon, and the energy of the scattered radiation is reduced. In an anti-Stokes event, the energy is transferred from the phonon to the radiation, which is thus increased in energy. In the figure,  $h$  is Planck's constant;  $\omega$  circular frequency,  $k$  photon wave vector,  $q$  phonon wave vector;  $\theta$  scattering angle;  $n$  refractive index;  $v_{th}$  acoustic velocity. (Figure courtesy of Hauke Marquardt)

spectrometer, to yield a spectrum of intensity against frequency, centred on the frequency of the incident light beam. Because most of the light that is incident upon the sample is scattered without exchanging energy with the acoustic vibrations or phonons (Rayleigh scattering), the spectrum is dominated by a peak at the frequency of the incident light. In a spectrum collected in a general orientation of a crystal there are three additional pairs of peaks, symmetrically present both at higher and lower frequencies than the incident light. These pairs correspond to the Stokes and anti-Stokes scattering from the three acoustic modes (Fig. 11). The difference in frequency of these peaks from the central Rayleigh peak is known as the Brillouin shift  $\Delta\omega_B$ . It depends on the wavelength of the incident laser light,  $\lambda_0$ , the refractive index  $n$  of the sample, the angle  $\theta$  between the incident and scattered light beams, and the acoustic wave velocity of the acoustic mode which has interacted with the light:

$$\Delta\omega_B = \pm \frac{4n\pi}{\lambda_0} v \sin\left(\frac{\theta}{2}\right) \quad (11)$$

The three pairs of peaks in the Brillouin spectrum (Fig. 11) from a single crystal correspond to the velocities of three mutually perpendicular polarizations of the acoustic waves. In general, one of the three modes will have a quasi-longitudinal character and the other two quasi-transverse characters. In fluids the only propagating acoustic waves will be longitudinal, so the spectrum will contain just a single pair of peaks from which the bulk modulus can be obtained directly through Equation (9). In elastically isotropic solids, such as a perfect polycrystalline aggregate, or a glass, the two shear modes have the same frequency, and thus only two pairs of peaks (one  $p$ - and one  $s$ -wave) appear in the spectrum, and the moduli are again obtained directly from

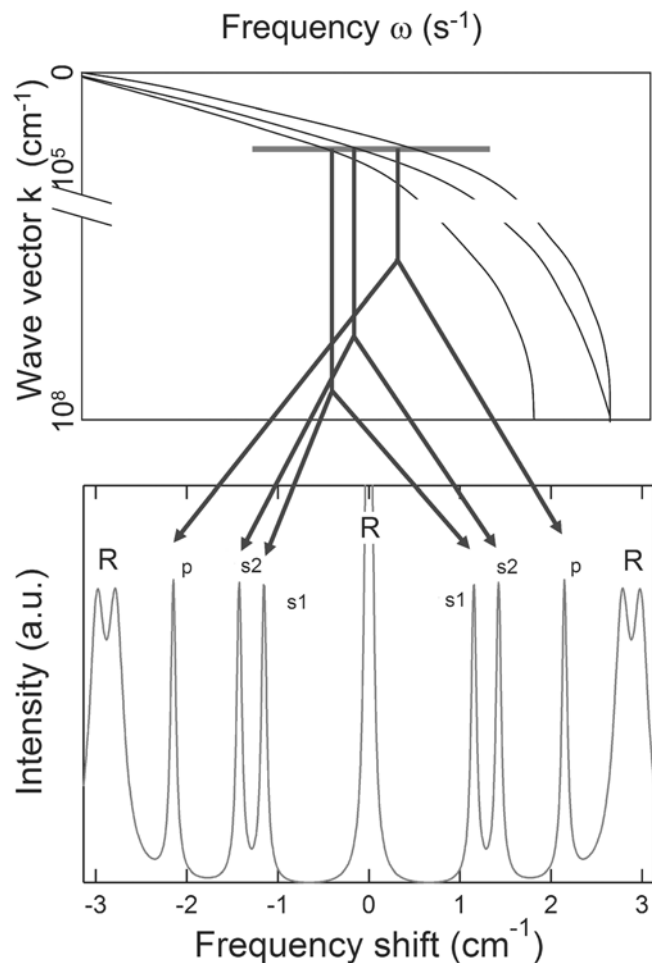


Fig. 11. Dispersion curves for the acoustic modes in a general direction of a single crystal, along with the Brillouin spectrum. The central strong peak, *R*, is the elastically scattered light peak (Rayleigh peak). The peaks *s1* and *s2* correspond to the slow and the fast shear acoustic modes respectively, and *p* to the longitudinal acoustic mode. Note that the higher frequency modes give rise to higher Brillouin shifts.

a single spectrum (Equation (8); *e.g.*, Cummins & Schoen, 1972; Sinogeikin *et al.*, 2004b; Murakami *et al.*, 2007a, b). For single crystal experiments, a large number of measurements of different acoustic waves must be made in different directions, which are selected from the knowledge of the scattering geometry. For this reason, most Brillouin experimental set-ups incorporate a goniometer with which the sample orientation can be changed systematically and precisely. The elastic moduli are obtained through Equation (7) by adjusting the values of the moduli in a least-squares process so as to match the observed velocities and propagation directions.

In order to determine the components of the elastic tensor of anisotropic solids, it is clearly important to know the orientation of the probed acoustic wave. This implies that the relative orientations of incident and scattered light beams and, consequently, of the scattering wave have to be determined. Knowledge of the refractive index of the medium is also required in the majority of the

experimental geometries (Kruger *et al.*, 1986; Grimsditch & Polian, 1989), which make them unsuitable for high-pressure measurements. However, in the symmetric forward scattering geometry knowledge of the refractive index of the medium is not required (Withfield *et al.*, 1976), because the wave vector of the acoustic wave is completely determined by the external angle between the incident and scattered beams outside the sample assembly (diamond-anvil or furnace, pressure transmitting medium, and sample). In this experimental geometry, the sample must be a plate whose faces must be parallel to within a few hundredths of degree (see discussion in Sinogeikin & Bass, 2000; Zha *et al.*, 2000).

The precision of the wave velocity measurement depends on the precision with which the Brillouin shifts can be measured. As these are typically of the order of  $1 \text{ cm}^{-1}$ , that is in the GHz frequency range, precision is obtained through optical interferometry. One of the most popular designs of Brillouin spectrometers is based on the multi-pass tandem Fabry-Perot interferometer (Sandercock, 1982). The combination of high-precision positioning of both the sample and the incident and receiving optics with high-resolution spectrometers makes it possible to obtain a precision of the order of 0.1 % in frequency shift and velocity. The accuracy to which the coefficients of the elastic tensor can be determined has been tested on standard materials and it can be as good as 1 % (Speziale & Duffy, 2002).

The great advantage of Brillouin scattering is that it can be measured on very small samples of only a few tens of micrometers in size, with typical sampling volumes of the same size. This makes it ideal for high-temperature measurements in furnaces (*e.g.*, Askarpour *et al.*, 1993; Jackson *et al.*, 2007) or laser heating (Sinogeikin *et al.*, 2004a, 2005) at ambient pressure, and is especially suited for high-pressure experiments with diamond-anvil cells. For high-symmetry crystals a single loading of a crystal is sufficient to determine the entire set of tensor components, provided several orientations are measured (*e.g.*, Speziale & Duffy, 2002), and measurements have been performed above 50 GPa at ambient temperature (Zha *et al.*, 2000; Shimizu *et al.*, 2001). Lower-symmetry crystals require either multiple loadings, or multiple crystals to be loaded together in order to provide the spatial coverage necessary to obtain all of the elastic moduli (*e.g.*, Zha *et al.*, 1996; Sinogeikin *et al.*, 2003). Polycrystalline aggregates can also be measured at high pressures in the diamond-anvil cell in order to obtain the bulk and shear moduli (Sinogeikin *et al.*, 2004b; Jackson *et al.*, 2005b; Murakami *et al.*, 2007a, b). Brillouin scattering has been recently measured at high pressure and temperatures up to 30 GPa and 600 °C by combining diamond-anvil cells with resistive heating (Sinogeikin *et al.*, 2007). There are very few limitations to Brillouin scattering. The only regime in which Brillouin scattering is not effective is at low temperatures, because the intensity of the scattered light falls as the thermally-induced vibrations of the atoms decrease. It is very difficult to use on optically opaque samples, especially in the DAC (Crowhurst *et al.*, 1999) because the scattering efficiency is

very low. And, while there is no reason why Brillouin spectroscopy cannot be used on samples of low symmetry, the number of measurements required to obtain sufficient data coverage means that the number of measurements on monoclinic minerals, even at room conditions, is very few (*e.g.*, Weidner & Carleton, 1977; Levien *et al.*, 1979; Kandelin & Weidner, 1988a, b). The authors are aware of only one full determination of the elastic tensor of a triclinic mineral by Brillouin scattering (Swanson, 1984).

#### 4.6. Momentum-resolved inelastic X-ray scattering (IXS)

The physical processes that underlie momentum-resolved inelastic scattering of X-rays (IXS) are similar to those described for inelastic scattering of light in Brillouin spectroscopy. The difference between IXS and Brillouin scattering lies in the particle probe. X-rays have shorter wavelengths ( $\lambda \sim 0.1$  nm) and therefore provide access to larger sections of the dispersion scheme. This is in contrast to inelastic light scattering methods such as Brillouin or Raman scattering that can only determine the acoustic and optic modes, respectively, at very long wavelengths (or small momentum transfers) close to the Brillouin zone centre. IXS investigations carried out on polycrystalline samples routinely provide orientationally averaged longitudinal acoustic velocities, whereas measurements on single-crystals provide single-crystal elastic moduli.

Synchrotron X-rays with a given energy and bandwidth interact with quantized lattice vibrations (phonons) in the sample and are inelastically scattered at a known angle (Fig. 10). Focus spot sizes are as low as 30  $\mu\text{m}$  (horizontal) by 10  $\mu\text{m}$  (vertical). The scattered photons are analysed by several analysers, which are mounted on a Rowland circle at a distance of several meters. The monochromator design, focus spot sizes, number of analysers, and sample-to-analyser distance varies depending on the instrument. At present, there are five instruments dedicated to IXS for the study of phonons: ID16 and ID28 at the European Synchrotron Radiation Facility in Grenoble (France), 3ID and 30ID at the Advanced Photon Source in the Chicago, IL area (USA), and BL35XU at the Super Photon Ring in Kansai (Japan). The reader is referred to Burkel (2001) and Krisch & Sette (2007) for details on the theoretical background and recent status of IXS.

If the sample is a single crystal, the directional dependence of the acoustic modes is obtained and, with a known density, the values of the elastic moduli  $c_{ij}$  can be determined (Equation (7)). In the cases where the sample is crystalline, the sample must be oriented on a Bragg reflection and selection rules apply. Probing phonon excitations using IXS requires a relatively high energy resolution of at least  $\Delta E/E = 10^{-7}$ . The acoustic modes are determined by probing their respective phonon dispersion curves close to the Brillouin zone centre (Fig. 9). Therefore, practical use of IXS to determine the sound velocities of materials has only been made possible in the last decade due to advances in X-ray optics and the advent of third-generation synchrotron sources. At a resolution of 1 meV, measurements are

feasible at high pressures on reasonable time scales of typically one pressure point per day.

Together with the extraction of the sound velocities and known density, the single-crystal elastic moduli may be determined with a high degree of accuracy. Aggregate elastic properties can also be obtained from polycrystalline samples, but these measurements are generally restricted to the longitudinal acoustic mode because the transverse modes yield lower signal to noise ratios (see Bosak *et al.*, 2007). A lower resolution ( $>1$  meV) can be employed if the studies are not aimed at obtaining sound velocities, but rather the general shape of the dispersion curve. In general, higher-resolution measurements require longer data collection times. IXS measurements can be performed on very small sample volumes ( $\sim 10^{-4}$  mm<sup>3</sup>) that can be optically transparent or opaque. The scattering cross-section is a function of absorption coefficient ( $\mu$ ), physical density, and probing energy. The optimal signal for DAC experiments is generally obtained if the absorption length ( $t = 1/\mu$ ) is of the order of 10–40  $\mu\text{m}$ , which span elements with  $Z$  between 30 and 50. However, IXS has proven to be successful for geophysically relevant samples in DACs with lower and higher  $Z$  (Sinn *et al.*, 2003; Antonangeli *et al.*, 2004; Fiquet *et al.*, 2004; Alatas *et al.*, 2005; Badro *et al.*, 2007; Kantor *et al.*, 2007).

#### 4.7. Inelastic neutron scattering (INS)

The processes involved in inelastic neutron scattering (INS) are similar to that of IXS (Fig. 10). In the case of INS, the probing particle is the neutron and one obtains the neutron-weighted phonon dispersion. Just as in IXS, the acoustic velocities are determined from the slope of the dispersion curves near the Brillouin zone centre, and the elastic constants can be calculated (*e.g.*, Boysen *et al.*, 1991; Artioli *et al.*, 1996). The energy of thermal neutrons that are on the order of inter-atomic distances is comparable to typical phonon energies ( $\sim 100$  meV) and the momentum of the neutron allows the whole dispersion scheme to be probed. For a recent review on the application of inelastic neutron scattering in the Earth sciences, the reader is referred to Loong (2006). Sample volumes must be of the order of several cubic millimetres (several grams) and this limits the pressures that can currently be achieved with INS. The method of INS, and its application to the high-pressure behaviour of minerals, will certainly prosper with commissioning and upgrading of several neutron sources: the Spallation Neutron Source at Oak Ridge National Laboratory (USA), the Neutron Arena of the J-PARC Project (Japan), and the second target station of ISIS at the Rutherford Appleton Laboratory (United Kingdom).

#### 4.8. Nuclear resonant inelastic X-ray scattering (NRIXS)

While conventional inelastic scattering techniques probe any lattice vibration in a crystal, nuclear resonant inelastic X-ray scattering is an inelastic scattering method that is

tuned to the resonance of a specific type of nuclei in the sample. NRIXS thus provides information about the lattice vibrations that involve only those nuclei. The resulting spectra can be processed to provide constraints on the partial phonon density of states involving those nuclei, from which values of the sound velocities (and hence moduli) of the sample can be determined. Because NRIXS signals originate from particular resonant nuclei only, it provides a unique selectivity among techniques for the study of lattice vibrations. For example, materials surrounding the sample that do not contain resonant nuclei produce no unwanted background, permitting experiments in extreme environments that were otherwise impossible. In the Earth sciences, the most common, abundant, and suitable nuclear resonant isotope is  $^{57}\text{Fe}$ . There are, however, other suitable isotopes that can be exploited for Earth science applications, including  $^{119}\text{Sn}$ ,  $^{161}\text{Dy}$ ,  $^{151}\text{Eu}$  and  $^{83}\text{Kr}$  (Sturhahn & Jackson, 2007).

For a comprehensive description of nuclear resonances and an overview of the nuclear resonant scattering field, the reader is referred to Sturhahn (2004) and the collection of review articles in Gerdau & de Waard (1999/2000). In simple terms, X-rays with the same energy as a difference between energy levels of the nucleus can be absorbed by the nucleus, which becomes excited. The nucleus therefore experiences a resonance. When the nucleus returns to the ground state, it emits an X-ray, whose energy is shifted with respect to the incident X-rays. This re-emission occurs on a timescale that is much longer than that of conventional Bragg (electronic) scattering of X-rays, and can thus be observed by exploiting of the pulsed nature of synchrotron sources and the very fast (nanoseconds) time resolution of detectors.

A schematic of the typical setup for nuclear resonant scattering experiments that is implemented at third-generation synchrotron radiation facilities is given elsewhere in this issue (Jackson *et al.*, 2009). For NRIXS

measurements, the energy bandwidth of the incident X-rays determines the resolution of the phonon spectra of the samples. The high-resolution monochromator is tuned around the nuclear transition energy with an energy bandwidth of about 1 meV or 0.24 THz (Toellner *et al.*, 2001). Focusing optics concentrate a significant portion of the X-ray beam into an area of less than  $10 \times 10 \mu\text{m}^2$  size at the sample. The incoherent radiation re-emitted by the sample is observed with an avalanche photo diode detector that is placed as close as possible to the sample but away from any strong coherent scattering directions, and the integrated delayed counting rate is recorded. The raw NRIXS spectra (Fig. 12) represent the intensity of the scattered radiation as a function of the energy shift from the resonance energy. NRIXS spectra, like Brillouin scattering spectra, consist of a Stokes and anti-Stokes portion, corresponding to energy gained and lost to the sample vibrations. If the resonant nuclei were fixed, there would be a single sharp peak in the spectrum located at the resonance energy (14.4125 keV for  $^{57}\text{Fe}$ ). The broader distribution is due to the fact that the nucleus is also involved in the atomic vibrations within the crystal. This distribution is then used to construct a phonon density of states (Fig. 12 and Sturhahn, 2000, 2004).

If the sample contains only the resonant nucleus (for example a sample of iron with 100%  $^{57}\text{Fe}$ ), then the phonon density of states calculated from the NRIXS spectra is complete (Fig. 12). Samples normally contain non-resonant atoms as well, as in  $^{57}\text{Fe}_2\text{O}_3$  hematite or  $^{57}\text{Fe}_{0.9}\text{Ni}_{0.1}$  alloy for example. In these cases, only the  $^{57}\text{Fe}$ -weighted partial PDOS is determined. However, because sound velocities correspond to vibrations of long wavelength (the acoustic modes close to the zone centre), the resonant nuclei participate in all of the acoustic modes, and the determination of the sound velocities is accurate for the bulk sample (Hu *et al.*, 2003; Sturhahn & Jackson, 2007).

The quantitative description of the low-energy region of the phonon DOS provides the Debye sound velocity,  $V_D$ .

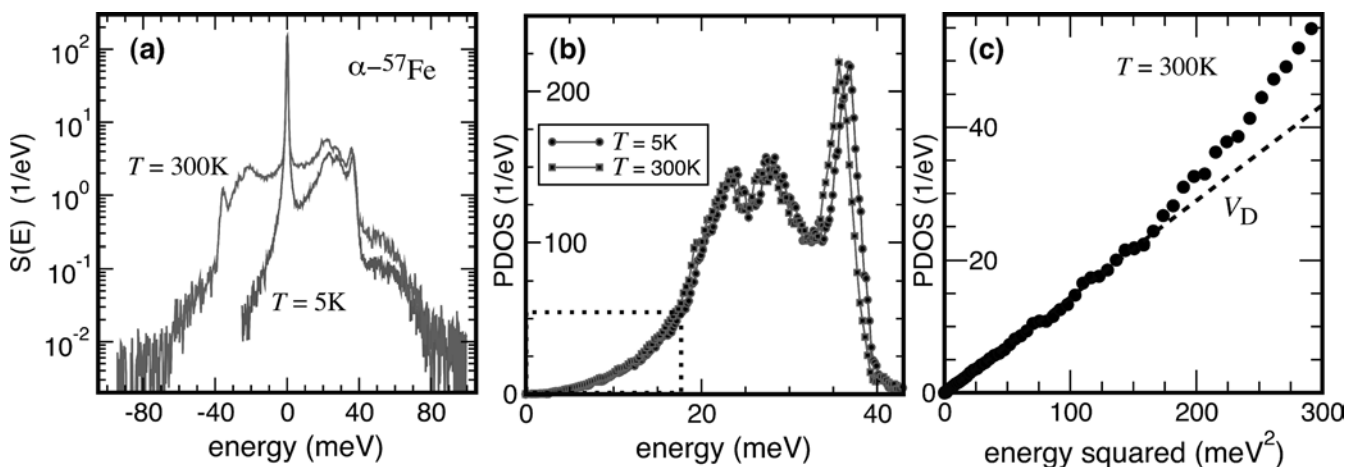


Fig. 12. Typical procedure for NRIXS data collection and analysis: (a) raw NRIXS spectra of polycrystalline  $\alpha$ -iron at 300 K and at 5 K, (b) extraction of the phonon density of states, and (c) the determination of the Debye sound velocity ( $V_D$ ). The decrease in intensity of the anti-Stokes scattering portion of the spectrum (left side, a) at low temperatures is due to the lower thermal vibrations in the crystal. The data points in (c) are taken from the PDOS within the dashed rectangle in (b) and are used to determine  $V_D$  (dashed straight line, c). Portions of this figure were adapted from Sturhahn (2004).

The derivation of the Debye sound velocity relies on a linear dispersion that will only be accurate within a limited energy range (Fig. 12). Therefore, it is not only important to have high-resolution data, it is also important to systematically evaluate errors resulting in selective energy ranges of the low-energy portion of the PDOS (see Sturhahn & Jackson, 2007, for a complete discussion of this error analysis). The Debye sound velocity is related to the compressional,  $V_P$ , and shear,  $V_S$ , velocities for an isotropic solid, using:

$$\left(\frac{3}{V_D^3}\right) = \left(\frac{1}{V_P^3}\right) + \left(\frac{2}{V_S^3}\right) \quad (12)$$

Combining Equation (12) with Equation (8) and  $V_\phi = (K_S/\rho)^{0.5}$ , one obtains the general solutions for  $V_S$  and  $V_P$ :  $V_S = 0.952V_D - 0.041V_\phi$  and  $V_P = 0.908V_\phi + 0.297V_D + 0.243V_D^2/V_\phi$ . One can see from Equation (12) that the Debye sound velocity is heavily weighted towards the shear sound velocity. Determination of sound velocities from NRIXS for geophysical applications has been successfully applied to pure iron (Mao *et al.*, 2001; Lin *et al.*, 2005), iron-alloys (Lin *et al.*, 2003, 2004b; Mao *et al.*, 2004; Gao *et al.*, 2008), silicates (Jackson *et al.*, 2009) and iron-bearing oxides and sulphides (Lin *et al.*, 2004a, 2006; Sturhahn & Jackson, 2007), with maximum pressures of 153 GPa at room temperature and 53 GPa at 1400 °C. Typical acquisition times for a NRIXS spectrum range between 1 h for iron-rich samples under ambient conditions and days for dilute and small samples under very high pressures.

## 5. Conclusions

All of the various experimental techniques for measuring the elasticity of minerals that we have discussed in the fore-going sections have specific advantages and disadvantages (Table 2), which should be considered when needing to determine the elasticity of a mineral. In general, measurements on polycrystalline materials (such as compacted powders) are much faster, and can be made at more extreme conditions of temperature and pressure, than when the same technique is applied to single-crystal samples. On the other hand, measurements of powders or polycrystalline aggregates normally only yield the bulk and shear moduli of the material, but not any information about the anisotropy of the elasticity. The one exception is high-pressure powder diffraction that yields the same sums of the components of the compliance tensor as single-crystal diffraction but, of course, provides no information about the shear modulus  $G$ .

The measurement of individual components of the elastic tensor with any method other than RUS requires multiple measurements to be performed on different directions on a single crystal, or set of single-crystal samples. The number of measurements that are required increases with lower symmetry, as more components of the elastic tensor have

to be determined (Table 1). Therefore, complete determinations of the elastic tensor of the monoclinic and triclinic minerals that are common in the Earth's crust (*e.g.*, pyroxenes, amphiboles and feldspars) are relatively few, as measurements by Brillouin spectroscopy, IXS, or ultrasonic interferometry take many weeks even at room conditions. The development of ISLS, which can be performed relatively rapidly on large samples at ambient conditions thus provides an opportunity to fill in this gap in our database on the elasticity of minerals. If sufficiently large crystals of suitable quality are available, then RUS provides the possibility of rapidly measuring the complete elastic tensor at many closely-spaced temperature steps to very high temperatures. The determination of the full elastic tensor of a low-symmetry crystalline sample at high pressures is a far more demanding undertaking, as it requires (whatever the technique) the measurement of many different directions within the sample, and thus multiple sample loadings. Thus we have seen that the majority of high pressure, and high  $P,T$ , measurements have focused on relatively high-symmetry materials such as MgO, Fe, etc., and the complete determination of the elastic tensor of, for example, MgSiO<sub>3</sub> perovskite at the pressures and temperatures of the Earth's lower mantle remains for the time being only tractable by computational methods.

The consistency that has been developed between different measurement techniques also allows them to be combined to provide either better-constrained results or more accurate ones. Methods to determine elasticity directly are often combined with diffraction measurements, so that the value of the density needed to convert wave velocities to elastic moduli does not have to be inferred from the elastic measurements alone. Similarly, diffraction measurements provide information on sample length for ultrasonic interferometry at high pressures. Different techniques also have different sensitivity to different combinations of elastic moduli, so precision in individual moduli can often be improved by combining techniques, as in ISLS with diffraction (Brown *et al.*, 2006). Given the difficulties in experimental measurements, computational methods also have a major role to play, for example in providing full elastic tensor determinations at pressures for which only bulk averaged data are available experimentally.

One of the other benefits of the development of consistency in the results obtained by different elasticity measurement techniques has been the start of work to develop an absolute pressure scale. The underlying principle is quite simple. If the volume of the material is measured at the same time as the bulk modulus, the compression curve can be constructed as a curve of bulk modulus against volume, *i.e.*  $K = f(V/V_0)$ . Integration of that experimentally-determined relationship then yields a pressure-volume curve, because the bulk modulus is defined as  $K = -V \partial P / \partial V$ . The result is then a practical and absolute pressure scale that relates both the density and the bulk modulus of the experimental material to the absolute pressure. All implementations of this idea require the compression of the sample to be measured, which is best accomplished by X-ray diffraction. Ultrasonic

Table 2. Comparison of techniques to measure elasticity.

Technique	Sample size	Poly/single crystal	$P$	$T$	$P$ & $T$	Frequency	Results	Comment
DMA	cm	Poly/Single	No	1000 °C	No	0.01–100 Hz	Combinations of $c_{ij}$ , anelastic response	Isothermal/adiabatic
Torsion	cm	Poly/Single	0.2 GPa	1500 °C	0.2 GPa/1500 °C	0.001–1 Hz	shear moduli, anelastic response	Isothermal/adiabatic, No compressional moduli
RUS	mm–cm	Poly Single	No	1500 °C	No	MHz	K, G, anelastic response Individual $c_{ij}$	Adiabatic, all $c_{ij}$ in one measurement
Diffraction	10–100 $\mu$ m	Poly Single	300 GPa 10 GPa	2700 °C	100 GPa/2700 °C 3 GPa/200 °C	0 Hz	K, sums of $s_{ij}$	Isothermal
Computation	–	Poly Single	Unlimited	Unlimited	Unlimited	0 Hz	K, G,	Isothermal
Ultrasonic interferometry	10 $\mu$ m – cm	Poly Single	20 GPa 10 GPa	1000 °C 700 °C	20 GPa/1300 °C 0.5 GPa/200 °C	MHz–GHz	individual $c_{ij}$	Adiabatic
ISLS	100 $\mu$ m – cm	Poly Single	120 GPa 17 GPa		5.5 GPa/400 °C	GHz	individual $c_{ij}$	Adiabatic
Brillouin	50 $\mu$ m – cm	Poly Single	170 GPa 50 GPa	1175 °C 2200 °C	30 GPa/600 °C	GHz	individual $c_{ij}$	Adiabatic
Inelastic X-ray scattering	10 $\mu$ m	Poly Single	150 GPa 40 GPa	2700 °C 700 °C	72 GPa/430 °C	THz	individual $c_{ij}$	Adiabatic
Inelastic neutron scattering	mm	Poly Single	3 GPa 0.5 GPa	1000 °C	No	THz	individual $c_{ij}$	Adiabatic
NRXS	10 $\mu$ m	Poly Single	153 GPa	1400 °C	53 GPa/1400 °C	THz	PDOS, G, Debye sound velocity	Adiabatic

Notes: The entries in the columns for pressure, temperature, and  $P$  &  $T$  combined, do not necessarily represent the limits to the technique, but only what has been achieved and reported in the published literature. The entries for the frequency represent the frequencies at which the response of the sample is probed; for inelastic methods, this is *not* the frequency of the probe radiation.

interferometry has been combined with X-ray diffraction in experiments employing a multi-anvil (Mueller *et al.*, 2003; Li *et al.*, 2006), Brillouin spectroscopy with diffraction from a sample in a DAC (Zha *et al.*, 2000; Bass *et al.*, 2006), and ultrasonic interferometry with single-crystal diffraction in a DAC (Reichmann *et al.*, 1998). However, such measurements are not quite complete, because the bulk modulus obtained from diffraction measurements is isothermal, whereas elasticity measurements yield adiabatic values. Until now, data reduction has assumed that the conversion factor ( $1 + \alpha\gamma T$ ) does not change with pressure; Spetzler & Yoneda (1993) have shown that if measurements are made over a range in temperature at each pressure, the conversion factor can be determined at high pressures.

We have tried to emphasize in this review the maturity, range and consistency of the techniques available for the measurement of the elastic tensors of crystals. The field has thus matured to the point where we can reasonably expect the database of the elasticity of major minerals to be completed (at least for room conditions) within the next few years. And measurements at higher pressures and temperatures will inevitably follow where required. The biggest challenges in elasticity will then be in two related areas; the time domain, and polyphase aggregates or rocks. Table 2 shows that currently available elasticity measurements span 16 orders of magnitude in the time-scales of processes that they probe in the sample; spectroscopies probe the vibrations of atoms at  $10^{13}$  Hz, whereas mechanical methods probe material properties on time scales up to 1–100 s. For crystals at ambient conditions and far from phase transitions, these various techniques remarkably measure the same elastic response. But at high temperatures, or in the neighbourhood of phase transitions, the results from different techniques diverge because the response of the sample is different on the different time scales. Thus, high-frequency techniques will still measure the “ideal” crystalline response, whereas slower probes will see softening associated with flow and relaxation of the sample, known as the *anelastic response*. This is often associated with the motion of twin walls or defects (*e.g.*, Harrison & Redfern, 2002; Harrison *et al.*, 2003), or the slip on boundaries between grains (Webb & Jackson, 2003; Jackson *et al.*, 2005a). Such processes are responsible for the seismic attenuation measured within the Earth, and could provide further constraints on both its mineralogy and the texture of rocks within the Earth.

Knowledge of the complete elastic tensor of a crystal allows the elastic (but not anelastic or plastic) properties of a polycrystalline aggregate of that mineral to be calculated. In rocks, there are additional variables; there are multiple types of boundaries between the grains of different phases, and the texture of the rock is also critically important. There is very little data on the elasticity of well-characterized “composites”, and much of it is for engineering composites involving fibres and inclusions. What is clear is that none of the available detailed models adequately explains the bulk elastic properties of aggregates in terms of their end-members (Shaocheng & Wang, 1999), even without the

issue of anelasticity. While Salje (2007) has indicated a possible way forward to estimating the elastic response of rocks, much remains to be done in the field of applying mineral physics data to the geology and geophysics of rocks.

**Acknowledgements:** This manuscript is based upon the lectures given by three of us at the International Mineralogical School on High-Pressure, High-Temperature Mineral Physics convened by the Gruppo Nazionale di Mineralogia and the *SIMP* of Italy. We would like to thank the organizing committee for the opportunity to present lectures to the school, and for providing funds that enabled our attendance. J. Kung, N.L. Ross, S. Webb, W. Sturhahn and Y. Yu provided information and advice while we were preparing this manuscript, and M.A. Carpenter, S. Jacobsen, F. Pandolfo and M. Parisatto are thanked for their thorough and constructive reviews. Work on the elasticity of minerals at Virginia Tech is supported by NSF grant EAR-0738692 to N.L. Ross and R.J. Angel, and at Caltech by NSF grant EAR-0711542 to J.M. Jackson.

## References

- Abramson, E.H. & Brown, J.M. (2004): Equation of state of water based on speeds of sound measured in the diamond-anvil cell. *Geochim. Cosmochim. Acta*, **68**, 1827–1835.
- Aizawa, Y., Barnhoorn, A., Faulz, U.H., Gerald, J.D.F., Jackson, I., Kovacs, I. (2008): Seismic properties of Anita Bay dunite: an exploratory study of the influence of water. *J. Petrol.*, **49**, 841–855.
- Alatas, A., Said, A.H., Sinn, H., Alp, E.E., Koditwakku, C.N., Reinhart, B., Saboungi, M.-L., Price, D.L. (2005): Elastic modulus measurements of supercooled liquid and hot solid silicon measured by inelastic x-ray scattering. *J. Phys. Chem. Solids*, **66**, 2230–2234.
- Anderson, O.L. (1995): Equations of state of solids for geophysics and ceramic science. Oxford University Press, Oxford, UK.
- Angel, R. (2000): Equations of state. in “High-Pressure and High-Temperature Crystal Chemistry”, R.M. Hazen & R.T. Downs, eds. *MSA Rev. Mineral. Geochem.* **41**, 35–60.
- Antonangeli, D., Ocellli, F., Requardt, H., Badro, J., Fiquet, G., Krisch, M. (2004): Elastic anisotropy in textured hcp-iron to 112 GPa from sound wave propagation measurements. *Earth. Planet. Sci. Lett.*, **225**, 243–251.
- Artioli, G., Pavese, A., Moze, O. (1996): Dispersion relations of acoustic phonons in pyrope garnet: Relationship between vibrational properties and elastic constants. *Am. Mineral.*, **81**, 19–25.
- Askarpour, V., Manghni, M.H., Fassbender, S., Yoneda, A. (1993): Elasticity of single-crystal  $\text{MgAl}_2\text{O}_4$  spinel up to 1273 K by Brillouin spectroscopy. *Phys. Chem. Miner.*, **19**, 511–519.
- Badro, J., Fiquet, G., Guyot, F., Gregoryanz, E., Ocellli, F., Antonangeli, D., d’Astuto, M. (2007): Effect of light elements on the sound velocities in solid iron: implications for the composition of Earth’s core. *Earth. Planet. Sci. Lett.*, **254**, 233–238.
- Bass, J.D., Sinogeikin, S.V., Lakshtanov, D.L., Prakapenka, V.B., Shen, G., Sanchez-Valle, C., Perillat, J., Wang, J. (2006): Brillouin scattering with simultaneous X-ray diffraction at

- GSCRS, advanced photon source: toward determination of absolute pressure scales. *Eos Trans. AGU*, **87**, MR52A-04.
- Birch, F. (1947): Finite elastic strain of cubic crystals. *Phys. Rev.*, **71**, 809–824.
- Bosak, A., Krisch, M., Fischer, I., Huotari, S., Monaco, G. (2007): Inelastic X-ray scattering from polycrystalline materials at low momentum transfer. *Phys. Rev. B*, **75**, 064106.
- Boysen, H., Frey, F., Schrader, H., Eckold, G. (1991): On the proto-ortho-/clinostatite phase transformation: single crystal x-ray and inelastic neutron investigation. *Phys. Chem. Minerals*, **17**, 629–635.
- Brown, J.M., Slutsky, L.J., Nelson, K.A., Cheng, L.-T. (1989): Single-crystal elastic constants of San Carlos peridot: an application of impulsive stimulated scattering. *J. Geophys. Res.*, **94**, 9485–9492.
- Brown, J.M., Abramson, E.H., Angel, R.J. (2006): Triclinic elastic constants for low albite. *Phys. Chem. Minerals*, **33**, 256–265.
- Burkel, E. (2001): Determination of phonon dispersion curves by means of inelastic X-ray scattering. *J. Phys. Condens. Matter*, **13**, 7627–7644.
- Carpenter, M.A. (2006): Elastic properties of minerals and the influence of phase transitions. *Am. Mineral.*, **91**, 229–246.
- Carpenter, M.A. & Salje, E.K.H. (1998): Elastic anomalies in minerals due to structural phase transitions. *Eur. J. Mineral.*, **10**, 693–812.
- Carpenter, M.A., Hemley, R.J., Mao, H.K. (2000): High-pressure elasticity of stishovite and the  $P4_2/mnm = Pnm$  phase transition. *J. Geophys. Res.*, **105**, 10807–10816.
- Chai, M. & Brown, J.M. (1996): Effects of static non-hydrostatic stress on the R lines of ruby. *Geophys. Res. Letts.*, **23**, 3539–3542.
- Chen, G., Liebermann, R.C., Weidner, D.J. (1998): Elasticity of single-crystal MgO to 8 Gigapascals and 1600 K. *Science*, **280**, 1913–1915.
- Chung, D.H. & Buessem, W.R. (1967): The Voigt-Reuss-Hill approximation and elastic moduli of polycrystalline MgO, CaF<sub>2</sub>, β-ZnS, ZnSe, and CdTe. *J. Appl. Phys.*, **38**, 2535–2540.
- Cook, R.K. (1957): Variation of elastic constants and static strains with hydrostatic pressure: a method for calculation from ultrasonic measurements. *J. Acous. Soc. Amer.*, **29**, 445–449.
- Crowhurst, J.C. & Zaug, J.M. (2004): Surface acoustic waves in germanium single crystals. *Phys. Rev. B*, **69**, 052301.
- Crowhurst, J.C., Hearne, G.R., Commins, J.D., Every, A.G., Stoddart, P.R. (1999): Surface Brillouin scattering at high pressure: application to a thin supported gold film. *Phys. Rev. B*, **60**, R14990–R14993.
- Crowhurst, J.C., Abramson, E.H., Slutsky, L.J., Brown, J.M., Zaug, J.M., Harrell, M.D. (2001): Surface acoustic waves in the diamond anvil cell: and application of impulsive stimulated light scattering. *Phys. Rev. B*, **64**, 100103.
- Crowhurst, J.C., Goncharov, A.F., Zaug, J.M. (2005): Direct measurement of the elastic properties of Fe and Co to 120 GPa – Implications for the composition of the Earth’s core. in “Frontiers in high pressure research for geophysical applications”, J. Chen, Y. Wang, T.S. Duffy, G. Shen, L.F. Dobrzhinetskaya, eds. Elsevier, 3–23.
- Crowhurst, J.C., Antonangeli, D., Brown, J.M., Goncharov, A.F., Farber, D.F., Aracne, C.M. (2006): Determination of the high pressure elasticity of cobalt from measured interfacial acoustic wave velocities. *Appl. Phys. Lett.*, **89**, 111920.
- Crowhurst, J.C., Brown, J.M., Goncharov, A.F., Jacobsen, S.D. (2008): Elasticity of (Mg,Fe)O through the spin transition of iron in the lower mantle. *Science*, **319**, 451–453.
- Cummins, H.Z. & Schoen, P.E. (1972): Linear scattering from thermal fluctuations. in “Laser handbook”, F.T. Arecchi & E.O. Schultz-DuBois, eds. North Holland Publishing Co., Amsterdam.
- Daraktchiev, M., Harrison, R.J., Mountstevens, E.H., Redfern, S.A.T. (2006): Effect of transformation twins on the anelastic behavior of polycrystalline Ca<sub>1-x</sub>Sr<sub>x</sub>TiO<sub>3</sub> and Sr<sub>x</sub>Ba<sub>1-x</sub>SnO<sub>3</sub> perovskite in relation to the seismic properties of Earth’s mantle perovskite. *Mater. Sci. Eng. A*, **442**, 199–203.
- Dove, M.T. (2003): Structure and dynamics: an atomic view of materials. Oxford University Press, Oxford, 334 p.
- Dubrovinskaia, N. & Dubrovinsky, L. (2003): Whole-cell heater for the diamond anvil cell. *Rev. Sci. Instrum.*, **74**, 3433–3437.
- Dubrovinsky, L. & Dubrovinskaia, N. (2004): Angle-dispersive diffraction under non-hydrostatic stress in diamond anvil cells. *J. Alloys Compd.*, **375**, 86–92.
- Every, A.G. & Briggs, G.A.D. (1998): Surface response of a fluid loaded solid to impulsive line and point forces: application to scanning acoustic microscopy. *Phys. Rev. B*, **58**, 1601–1612.
- Every, A.G., Kim, K.Y., Maznev, A.A. (1997): The elastodynamic response of a semi-infinite anisotropic solid to sudden surface loading. *J. Acous. Soc. Amer.*, **102**, 1346–1355.
- Fei, Y. & Wang, Y. (2000): High-pressure and high-temperature powder diffraction. in “High-Temperature and High-Pressure Crystal Chemistry”, R.M. Hazen & R.T. Downs, eds. MSA, Chantilly, VA, *Rev. Mineral. Geochem.*, **41**, 521–557.
- Fiquet, G., Badro, J., Guyot, F., Bellin, C., Krisch, M., Antonangeli, D., Requardt, H., Mermut, A., Farber, D., Aracne-Ruddle, C., Zhang, J. (2004): Application of inelastic X-ray scattering to the measurements of acoustic wave velocities in geophysical materials at very high pressure. *Phys. Earth Planet. Int.*, **143–144**, 5–18.
- Gao, L., Chen, B., Wang, J., Alp, E.E., Zhao, J., Lerche, M., Sturhahn, W., Scott, H., Huang, F., Ding, Y., Sinogeikin, S.V., Lundstrom, C.C., Bass, J.D., Li, J. (2008): Pressure-induced magnetic transition and sound velocities of Fe<sub>3</sub>C: implications for carbon in the Earth’s inner core. *Geophys. Res. Letts.*, **35**, GL034817.
- Gerdau, E. & Waard, H. (1999/2000): Nuclear resonant scattering of synchrotron radiation. *Hyperfine Interact.*, **123–125**.
- Grimsditch, M. & Polian, A. (1989): Brillouin scattering at high pressures. in “Simple molecular systems at very high density”, A. Polian, P. Loubeyre, N. Boccara, eds. Plenum, New York, 237–255.
- Gwanmesia, G.D., Zhang, J., Darling, K., Kung, J., Li, B., Wang, L., Neuville, D., Liebermann, R.C. (2006): Elasticity of polycrystalline (Mg<sub>3</sub>Al<sub>2</sub>Si<sub>3</sub>O<sub>12</sub>) to 9 GPa and 1000°C. *Phys. Earth Planet. Int.*, **155**, 179–190.
- Hackwell, T.P. & Angel, R.J. (1995): Reversed brackets for the P-I-I transition in anorthite at high-pressures and temperatures. *Am. Mineral.*, **80**, 239–246.
- Harrison, R.J. & Redfern, S.A. (2002): The influence of transformation twins on the seismic-frequency elastic and anelastic properties of perovskite: dynamical mechanical analysis of single crystal LaAlO<sub>3</sub>. *Phys. Earth Planet. Int.*, **134**, 253–272.
- Harrison, R.J., Redfern, S.A.T., Street, J. (2003): The effect of transformation twins on the seismic-frequency mechanical properties of polycrystalline Ca<sub>1-x</sub>Sr<sub>x</sub>TiO<sub>3</sub> perovskite. *Am. Mineral.*, **88**, 574–582.
- Harrison, R.J., Redfern, S.A.T., Bismayer, U. (2004a): Seismic-frequency attenuation at first-order phase transitions: dynamical mechanical analysis of pure and Ca-doped lead orthophosphate. *Mineral. Mag.*, **68**, 839–852.

- Harrison, R.J., Redfern, S.A.T., Buckley, A., Salje, E.K.H. (2004b): Application of real-time, stroboscopic x-ray diffraction with dynamical mechanical analysis to characterize the motion of ferroelastic domain walls. *J. Appl. Phys.*, **95**, 1706–1717.
- Harrison, R.J., Redfern, S.A.T., Salje, E.K.H. (2004c): Dynamical excitation and anelastic relaxation of ferroelastic domain walls in  $\text{LaAlO}_3$ . *Phys. Rev. B*, **69**, 144101–1441010.
- Hazen, R.M. & Downs, R.T. (2000): High-pressure and high-temperature crystal chemistry. *Rev. Mineral. Geochem.*, **41**. Mineralogical Society of America.
- Hu, M.Y., Sturhahn, W., Toellner, T.S., Mannheim, P.D., Brown, D.E., Zhao, J., Alp, E.E. (2003): Measuring velocity of sound with nuclear resonant inelastic X-ray scattering. *Phys. Rev. B*, **67**, 094304.
- Isaak, D.G., Carnes, J.D., Anderson, O.L., Cynn, H., Hake, E. (1998a): Elasticity of  $\text{TiO}_2$  rutile to 1800K. *Phys. Chem. Minerals.*, **26**, 31–43.
- Isaak, D.G., Carnes, J.D., Anderson, O.L., Oda, H. (1998b): Elasticity of fused silica spheres under pressure using resonant ultrasound spectroscopy. *J. Acous. Soc. Amer.*, **104**, 2200–2206.
- Isaak, D.G. & Ohno, I. (2003): Elastic constants of chrome-diopside: application of resonant ultrasound spectroscopy to monoclinic single-crystals. *Phys. Chem. Minerals.*, **30**, 430–439.
- Jackson, I. & Niesler, H. (1982): The elasticity of periclase to 3 GPa and some geophysical implications. in “High Pressure Research in Geophysics”, S. Akimoto and M.H. Manghnani, eds. Center for Academic Publications, Japan, *Adv. Earth Plan. Sci.*, 93–113.
- Jackson, I. & Paterson, M.S. (1993): A high-pressure high-temperature apparatus for studies of seismic wave dispersion and attenuation. *PAGEOPH*, **141**, 445–466.
- Jackson, I., Webb, S., Weston, L., Boness, D. (2005a): Frequency dependence of elastic wave speeds at high temperature: a direct experimental demonstration. *Phys. Earth Planet. Int.*, **148**, 85–96.
- Jackson, J.M., Zhang, J., Shu, J., Sinogeikin, S.V., Bass, J.D. (2005b): High-pressure sound velocities and elasticity of aluminous  $\text{MgSiO}_3$  perovskite to 45 GPa: implications for lateral heterogeneity in Earth’s lower mantle. *Geophys. Res. Lett.*, **32**, 023522.
- Jackson, J.M., Sinogeikin, S.V., Bass, J.D. (2007): Sound velocities and single-crystal elasticity of orthoenstatite to 1073 K at ambient pressure. *Phys. Earth Planet. Int.*, **161**, 1–12.
- Jackson, J.M., Hamecher, E.A., Sturhahn, W. (2009): Nuclear resonant X-ray spectroscopic study on  $(\text{Mg,Fe})\text{SiO}_3$  orthoenstatites. *Eur. J. Mineral.*, DOI: 10.1127/0935-1221/2009/0021-1932.
- Jacobsen, S.D., Reichmann, H.-J., Spetzler, H.A., Mackwell, S.J., Smyth, J.R., Angel, R.J., McCammon, C.A. (2002): Structure and elasticity of single-crystal  $(\text{Mg,Fe})\text{O}$  and a new method of generating shear waves for gigahertz ultrasonic interferometry. *J. Geophys. Res.*, **107**, 2001JB000490.
- Jacobsen, S.D., Smyth, J.R., Spetzler, H.A., Holl, C.M., Frost, D.J. (2004): Sound velocities and elastic constants of iron-bearing hydrous ringwoodite. *Phys. Earth Planet. Int.*, **143–144**, 47–56.
- Johnson, E. (2007): The elastic behavior of plagioclase feldspar at high pressure. Geosciences, MS Thesis, 121 p. Virginia Tech, Blacksburg VA.
- Jung, D.Y. & Oganov, A.R. (2005): Basics of first-principles simulation of matter. in “Mineral Behaviour at Extreme Conditions”, R. Miletich, ed., Eotvos University Press, Budapest. *EMU Notes Mineral.*, **7**, 117–138.
- Kandelin, J. & Weidner, D.J. (1988a): Elastic properties of hedenbergite. *J. Geophys. Res.*, **93**, 1063–1072.
- , — (1988b): The single-crystal elastic properties of jadeite. *Phys. Earth Planet. Int.*, **50**, 251–260.
- Kantor, A.P., Jacobsen, S.D., Kantor, I.Y., Dubrovinsky, L., McCammon, C.A., Reichmann, H.J., Goncharenko, I.N. (2004): Pressure-induced magnetization in FeO: Evidence from elasticity and Mössbauer spectroscopy. *Phys. Rev. Lett.*, **93**, 93215502.
- Kantor, A.P., Kantor, I.K., Kurnosov, A.V., Kuznetsov, A.Y., Dubrovinskaia, N.A., Krisch, M., Bossak, A.A., Dmitriev, V.P., Urusov, V.S., Dubravinsky, L. (2007): Sound wave velocities of fcc Fe-Ni alloy at high pressure and temperatures by mean of inelastic x-ray scattering. *Phys. Earth Planet. Int.*, **164**, 83–89.
- Karki, B.B., Stixrude, L., Wentzcovitch, R.M. (2001): High-pressure elastic properties of major materials of Earth’s mantle from first principles. *Rev. Geophys.*, **39**, 507–534.
- Keppeler, H. & Frost, D.J. (2005): Introduction to minerals under extreme conditions. in “Mineral Behaviour at Extreme Conditions”, R. Miletich, ed., Eotvos University Press, Budapest. *EMU Notes Mineral.*, **7**, 1–30.
- Kern, H. & Tubia, J. (1993): Pressure and temperature dependence of *p*- and *s*- wave velocities, seismic anisotropy and density of sheared rocks from the Sierra Alpujata massif (Ronda peridotites, Southern Spain). *Earth. Planet. Sci. Lett.*, **119**, 191–205.
- Krisch, M. & Sette, F. (2007): Inelastic X-ray scattering from phonons. in “Light scattering in solid IX”, M. Cardona & R. Merlin, eds. Springer-Verlag Berlin, Heidelberg, **108**, 317–370.
- Kruger, J.K., Marx, A., Peetz, L., Roberts, R., Unruh, H.G. (1986): Simultaneous determination of elastic and optical properties of polymers by high performance Brillouin spectroscopy using different scattering geometries. *Colloid. Polym. Sci.*, **264**, 403–414.
- Kung, J., Angel, R.J., Ross, N.L. (2001): Elasticity of  $\text{CaSnO}_3$  perovskite. *Phys. Chem. Minerals*, **28**, 35–43.
- Kung, J., Li, B., Weidner, D.J., Zhang, J., Liebermann, R.C. (2002): Elasticity of  $(\text{Mg}_{0.83}\text{Fe}_{0.17})\text{O}$  ferropericlase at high pressure: ultrasonic measurements in conjunction with X-radiation techniques. *Earth. Planet. Sci. Lett.*, **203**, 557–566.
- Levien, L., Weidner, D.J., Prewitt, C.T. (1979): Elasticity of diopside. *Phys. Chem. Minerals*, **4**, 105–113.
- Li, B. (2003): Compressional and shear wave velocities of ringwoodite  $\gamma\text{-Mg}_2\text{SiO}_4$  to 12 GPa. *Am. Mineral.*, **88**, 1312–1317.
- Li, B. & Zhang, J. (2005): Pressure and temperature dependence of elastic wave velocity of  $\text{MgSiO}_3$  perovskite and the composition of the lower mantle. *Phys. Earth Planet. Int.*, **151**, 143–154.
- Li, B., Liebermann, R.C., Weidner, D.J. (1998): Elastic moduli of wadsleyite ( $\beta\text{-Mg}_2\text{SiO}_4$ ) to 7 GPa and 873 K. *Science*, **281**, 675–677.
- Li, B., Chen, K., Kung, J., Liebermann, R.C., Weidner, D.J. (2002): Sound velocity measurements using transfer function method. *J Phys. Condens. Matter*, **14**, 11337–11342.
- Li, B., Woody, K., Kung, J. (2006): Elasticity of MgO to 11 GPa with an independent absolute pressure scale: Implications for pressure calibration. *J. Geophys. Res.*, **B111**, 11206.
- Lin, J.F., Struzhkin, V.V., Sturhahn, W., Huang, E., Zhao, J.Y., Hu, M.Y., Alp, E.E., Mao, H.K., Boctor, N., Hemley, R.J. (2003): Sound velocities of iron-nickel and iron-silicon alloys at high pressures. *Geophys. Res. Lett.*, **30**, 2112, DOI:10.1029/2003GL018405.

- Lin, J.-F., Fei, Y., Sturhahn, W., Zhao, J., Mao, H.-K., Hemley, R.J. (2004a): Magnetic transition and sound velocities of  $\text{Fe}_3\text{S}$  at high pressure: Implications for Earth and planetary cores. *Earth. Planet. Sci. Lett.*, **226**, 33–40.
- Lin, J.F., Sturhahn, W., Zhao, J.Y., Shen, G.Y., Mao, H.K., Hemley, R.J. (2004b): Absolute temperature measurement in a laser-heated diamond anvil cell. *Geophys. Res. Lett.*, **31**, L134611, DOI:10.1029/2003GL020599.
- , —, —, —, — (2005): Sound velocities of hot dense iron: Birch's law revisited. *Science*, **308**, 1892–1894.
- Lin, J.-F., Jacobsen, S.D., Sturhahn, W., Jackson, J.M., Zhao, J., Yoo, C.-S. (2006): Sound velocities of ferropicrinite in the Earth's lower mantle. *Geophys. Res. Lett.*, **33**, L22304, doi:10.1029/2006GL028099.
- Loong, C.-K. (2006): Inelastic scattering and applications. in "Neutron Scattering in Earth Sciences", H.-R. Wenk & J.J. Rosso, eds. The Mineralogical Society of America, Chantilly, VA, *Rev. Mineral. Geochem.*, **63**, 233–254.
- Mao, H.K., Xu, J., Struzhkin, V.V., Shu, J., Hemley, R.J., Sturhahn, W., Hu, M.Y., Alp, E.E., Vocadlo, L., Alfe, D., Price, G.D., Gillan, M.J., Schworer-Bohning, M., Hausermann, D., Eng, P., Shen, G., Giefers, H., Lubbers, R., Wortmann, G. (2001): Phonon density of states of iron up to 153 Gigapascals. *Science*, **292**, 914–916.
- Mao, W.L., Sturhahn, W., Heinz, D.L., Mao, H.K., Shu, J.F., Hemley, R.J. (2004): Nuclear resonant x-ray scattering of iron hydride at high pressure. *Geophys. Res. Lett.*, **31**, L15618, doi:10.1029/2004GL020541.
- Maznev, A.A., Akthakul, A., Nelson, K.A. (1999): Surface acoustic modes in thin films on anisotropic substrates. *J. Appl. Phys.*, **86**, 2818–2824.
- McKnight, R.E.A., Carpenter, M.A., Darling, T.W., Buckley, A., Taylor, P.A. (2007): Acoustic dissipation associated with phase transitions in lawsonite,  $\text{CaAl}_2\text{Si}_2\text{O}_7(\text{OH})_2 \cdot \text{H}_2\text{O}$ . *Am. Mineral.*, **92**, 1665–1672.
- Migliori, A. & Maynard, J.D. (2005): Implementation of a modern resonant ultrasound spectroscopy system for the measurement of the elastic moduli of small solid specimens. *Rev. Sci. Instrum.*, **76**, 121301.
- Mueller, H.J., Schilling, F.R., Lauterjung, J., Lathe, C. (2003): A standard-free pressure calibration using simultaneous XRD and elastic property measurements in a multi-anvil device. *Eur. J. Mineral.*, **15**, 865–873.
- Mueller, H.J., Lathe, C., Schilling, F.R. (2005a): Simultaneous determination of elastic and structural properties under simulated mantle conditions using multi-anvil device MAX80. in "Advances in high-pressure technology for geophysical applications", J. Chen, Y. Wang, T.S. Duffy *et al.*, eds. Elsevier, Amsterdam, 67–74.
- Mueller, H.J., Schilling, F.R., Lathe, C., Lauterjung, J. (2005b): Calibration based on a primary pressure scale. in "Advances in High-Pressure Technology For Geophysical Applications", J. Chen, Y. Wang, T.S. Duffy, eds. Elsevier, Amsterdam, 427–449.
- Murakami, M., Sinogeikin, S.V., Bass, J.D., Sata, N., Ohishi, Y., Hirose, K. (2007a): Sound velocity of  $\text{MgSiO}_3$  post-perovskite phase: a constraint on the  $D''$  discontinuity. *Earth. Planet. Sci. Lett.*, **259**, 18–23.
- Murakami, M., Sinogeikin, S.V., Hellwig, H., Bass, J.D., Li, J. (2007b): Sound velocity of  $\text{MgSiO}_3$  perovskite to Mbar pressure. *Earth. Planet. Sci. Lett.*, **256**, 47–54.
- Nasch, P.M., Manghanni, M.H., Secco, R.A. (1994): Sound velocity measurements in liquid iron by ultrasonic interferometry. *J. Geophys. Res.*, **B99**, 4285–4291.
- Nye, J.F. (1957): Physical properties of crystals. Oxford University Press, Oxford, 322 p.
- Oda, H., Anderson, O.L., Isaak, D.G., Suzuki, I. (1992): Measurement of elastic properties of single-crystal CaO up to 1200 K. *Phys. Chem. Minerals*, **19**, 96–105.
- Ohno, I., Harada, K., Yoshitomi, C. (2006): Temperature variation of elastic constants of quartz across the alpha-beta transition. *Phys. Chem. Minerals*, **33**, 1–9.
- Reichmann, H.J. & Jacobsen, S.D. (2006): Sound wave velocities and elastic constants of  $\text{ZnAl}_2\text{O}_4$  spinel and implications for spinel-elasticity systematics. *Am. Mineral.*, **91**, 1049–1054.
- Reichmann, H.J., Angel, R.J., Spetzler, H.A., Bassett, W.A. (1998): Ultrasonic interferometry and X-ray measurements on MgO in a diamond anvil cell. *Am. Mineral.*, **83**, 1357–1360.
- Reuss, A. (1929): Berechnung der Fließgrenze von Mischkristallen auf Grund der Konstanten des Einkristalls. *Zeit. Angew. Math. Mech.*, **9**, 49–58.
- Ross, N.L. & Hoffmann, C. (2006): Single-crystal neutron diffraction: present and future applications. in "Neutron Scattering in Earth Sciences", H.-R. Wenk, ed. MSA, Chantilly, VA, **63**, 59–80.
- Salje, E.K.H. (2007): An empirical scaling model for averaging elastic properties including interfacial effects. *Am. Mineral.*, **92**, 429–432.
- Sandercock, J.R. (1982): Trends in Brillouin scattering: studies of opaque materials, supported films, and central modes. in "Light scattering in solids III: recent results, topics in applied physics", M. Cardona & G. Guntherodt, eds. Springer Verlag, Berlin, 173–206.
- Schranz, W. (1997): Dynamic mechanical analysis - a powerful tool for the study of phase transitions. *Phase Transitions*, **64**, 103–114.
- Schreuer, J. & Haussühl, S. (2005): Elastic and piezoelectric properties of minerals I. principles and experimental approaches. in "Mineral Behaviour at Extreme Conditions", R. Miletich, ed. Eotvos University Press, Budapest, *EMU Notes Mineral.*, **7**, 173–198.
- Shaocheng, J. & Wang, Z. (1999): Elastic properties of forsterite-enstatite composites up to 3.0 GPa. *Geodynamics*, **28**, 147–174.
- Shimizu, H., Tashiro, H., Kume, T., Sasaki, S. (2001): High-pressure properties of solid argon to 70 GPa. *Phys. Rev. Lett.*, **86**, 4568–4571.
- Singh, A.K., Mao, H.K., Shu, J.F., Hemley, R.J. (1998): Estimation of single-crystal elastic moduli from polycrystalline X-ray diffraction at high pressure: application to FeO and iron. *Phys. Rev. Lett.*, **80**, 2157–2160.
- Sinn, H., Glorieux, B., Hennet, L., Alatas, A., Hu, M., Alp, E.E., Bermejo, F.J., Price, D.L., Saboungi, M.-L. (2003): Microscopic dynamics of liquid aluminum oxide. *Science*, **299**, 2047–2049.
- Sinogeikin, S.V. & Bass, J.D. (2000): Single-crystal elasticity of pyrope and MgO to 20 GPa by Brillouin scattering in the diamond cell. *Phys. Earth Planet. Int.*, **120**, 43–62.
- Sinogeikin, S.V., Bass, J.D., Katsura, T. (2003): Single-crystal elasticity of ringwoodite to high pressures and high temperatures: implications for the 520 km seismic discontinuity. *Phys. Earth Planet. Int.*, **136**, 41–66.
- Sinogeikin, S.V., Lakshtanov, D.L., Nicholas, J.D., Bass, J.D. (2004a): Sound velocity measurements on laser-heated MgO and  $\text{Al}_2\text{O}_3$ . *Phys. Earth Planet. Int.*, **143**, 575–586.
- Sinogeikin, S.V., Zhang, J.Z., Bass, J.D. (2004b): Elasticity of single crystal and polycrystalline  $\text{MgSiO}_3$  perovskite by Brillouin spectroscopy. *Geophys. Res. Lett.*, **31**, doi:10.1029/2004GL019559.

- Sinogeikin, S.V., Lakshtanov, D.L., Nicholas, J.D., Jackson, J.M., Bass, J.D. (2005): High temperature elasticity measurements on oxides by Brillouin spectroscopy with resistive and IR laser heating. *J. Eur. Ceram. Soc.*, **25**, 1313–1324.
- Sinogeikin, S.V., Lakshtanov, D.L., Prakapenka, V.B., Sanchez-Valle, C., Wang, J., Chen, B., Shen, G., Bass, J.D. (2007): Toward a self-consistent pressure scale: elastic moduli and equation of state of MgO by simultaneous x-ray density and Brillouin sound velocity measurements at high-pressure high-temperature conditions. *Eos Trans., AGU, Fall Meet. Suppl.*, **88**, Abstract MR53A-07.
- Spetzler, H.A. & Yoneda, A. (1993): Performance of the complete travel-time equation of state at simultaneous high pressure and temperature. *PAGEOPH*, **141**, 379–392.
- Spetzler, H.A., Chen, G., Whitehead, S., Getting, I.C. (1993): A new ultrasonic interferometer for the determination of equation of state parameters of sub-millimeter single crystals. *PAGEOPH*, **141**, 341–377.
- Spetzler, H., Shen, A., Chen, G., Herrmannsdörfer, G., Schulze, H., Weigel, R. (1996): Ultrasonic measurement in a diamond anvil cell. *Phys. Earth Planet. Int.*, **98**, 93–99.
- Speziale, S. & Duffy, T.S. (2002): Single-crystal elastic constants of fluorite (CaF<sub>2</sub>) to 9.3 GPa. *Phys. Chem. Miner.*, **29**, 465–472.
- Speziale, S., Shieh, S.R., Duffy, T.S. (2006): High pressure elasticity of calcium oxide: A comparison between Brillouin spectroscopy and radial X-ray diffraction. *J. Geophys. Res.*, **111**, B02203.
- Stixrude, L., Cohen, R.E., Hemley, R.J. (1998): Theory of minerals at high pressures. in “Ultra-high pressure mineralogy: physics and chemistry of the Earth’s deep interior”, R.J. Hemley, ed. M.S.A., Washington DC, 37
- Sturhahn, W. (2000): CONUSS and PHOENIX: evaluation of nuclear resonant scattering data. *Hyperfine Interact.*, **125**, 149–172.
- (2004): Nuclear resonant spectroscopy. *J. Phys. Condens. Matter*, **16**, S497–S530.
- Sturhahn, W. & Jackson, J.M. (2007): Geophysical applications of nuclear resonant spectroscopy. in “Advances in High-Pressure Mineralogy”, E. Ohtani, ed. The Geological Society of America, **421**, 157–174.
- Swanson, D. (1984): High-temperature crystal chemical formalism applied to K<sub>2</sub>Si<sup>VI</sup>Si<sub>3</sub><sup>IV</sup>O<sub>9</sub> and NaGaSi<sub>3</sub>O<sub>8</sub>. Department of Earth Sciences, PhD. Thesis, SUNY at Stony Brook, Stony Brook, NY.
- Toellner, T.S., Hu, M.Y., Sturhahn, W., Bortel, G., Alp, E.E., Zhao, J. (2001): Crystal monochromator with a resolution beyond 10<sup>8</sup>. *J. Synchr. Rad.*, **8**, 1082–1086.
- Uchida, T., Funamori, N., Yagi, T. (1996): Lattice strains in crystals under uniaxial stress field. *J. Appl. Phys.*, **80**, 739–746.
- Vanpeteghem, C.B., Zhao, J., Angel, R.J., Ross, N.L., Bolfan-Casanova, N. (2006): Crystal structure and equation of state of MgSiO<sub>3</sub> perovskite. *Geophys. Res. Lett.*, **33**, 024955.
- Vaughan, M., Chen, J., Li, L., Weidner, D.J., Li, B. (2000): Use of X-ray image techniques at high pressure and temperature for strain measurements. in “Science and technology of high pressure”, M.H. Manghnani, W.J. Nellis, M.F. Nicol, eds. Hyderabad University Press, Hyderabad, 1097–1098.
- Voigt, W. (1928): *Lehrbuch der Kristallphysik*. Tuebner, Berlin.
- Wallace, D.C. (1972): *Thermodynamics of Crystals*. Wiley, Hoboken, NJ, USA.
- Walsh, J.W., Taylor, P.A., Buckley, A., Darling, T.W., Schreuer, J., Carpenter, M.A. (2008): Elastic and anelastic anomalies in (Ca,Sr)TiO<sub>3</sub> perovskites: analogue behaviour for silicate perovskites. *Phys. Earth Planet. Int.*, **167**, 110–117.
- Webb, S.L. (1989): The elasticity of the upper mantle orthosilicates olivine and garnet to 3 GPa. *Phys. Chem. Minerals*, **16**, 684–692.
- (2005): Viscoelasticity of the Earth’s mantle. in “Mineral Behaviour at Extreme Conditions”, R. Miletich, ed., Eotvos University Press, Budapest. *EMU Notes Mineral.*, **7**, 417–440.
- Webb, S. & Courtial, P. (1996): Compressibility of P<sub>2</sub>O<sub>5</sub> - Al<sub>2</sub>O<sub>3</sub> - Na<sub>2</sub>SiO<sub>3</sub> melts. *Phys. Chem. Minerals*, **23**, 205–211.
- Webb, S.L. & Dingwell, D.B. (1994): Compressibility of titanosilicate melts. *Contrib. Mineral. Petrol.*, **118**, 157–168.
- , — (1995): Viscoelasticity. in “Structure, Dynamics and Properties of Silicate Melts”, J.F. Stebbins, P.F. McMillan, D.B. Dingwell, eds. *MSA Rev. Mineral. Geochem.*, **32**, 95–119.
- Webb, S. & Jackson, I. (2003): Anelasticity and microcreep in polycrystalline MgO at high temperature: an exploratory study. *Phys. Chem. Minerals*, **30**, 157–166.
- Webb, S., Jackson, I., Fitz Gerald, J.D. (1999): Viscoelasticity of the titanate perovskites CaTiO<sub>3</sub> and SrTiO<sub>3</sub> at high temperature. *Phys. Earth Planet. Int.*, **115**, 259–291.
- Weidner, D.J. & Carleton, H.R. (1977): Elasticity of coesite. *J. Geophys. Res.*, **82**, 1334–1346.
- Weidner, D.J., Li, L., Davis, M., Chen, J. (2004): Effect of plasticity on elastic modulus measurements. *Geophys. Res. Lett.*, **31**, L06621.
- Wentzcovitch, R.M., Martins, J.L., Price, G.D. (1993): Ab-initio molecular dynamics with variable cell-shape - application to MgSiO<sub>3</sub>. *Phys. Rev. Lett.*, **70**, 3947–3950.
- Wentzcovitch, R.M., Karki, B.B., Cococcioni, M., Gironcoli, S.D. (2004): Thermoelastic properties of MgSiO<sub>3</sub>-perovskite: insights into the nature of the Earth’s lower mantle. *Phys. Rev. Lett.*, **92**, 018501.
- Withfield, C.H., Brody, E.M., Bassett, W.A. (1976): Elastic moduli of NaCl by Brillouin scattering at high pressure in a diamond-anvil cell. *Rev. Sci. Instrum.*, **47**, 942–947.
- Yoneda, A. (1990): Pressure derivatives of elastic constants of single crystal MgO and MgAl<sub>2</sub>O<sub>4</sub>. *J. Phys. Earth*, **38**, 19–55.
- Yu, Y.G. & Wentzcovitch, R.M. (2006): Density functional study of vibrational and thermodynamic properties of ringwoodite. *J. Geophys. Res.*, **111**, B12202, doi:10.1029/2006JB004282.
- Zaug, J.M., Abramson, E.H., Brown, J.M., Slutsky, L.J. (1992): Elastic constants, equations of state and thermal diffusivity at high pressure. in “High pressure research: applications to Earth and planetary sciences”, Y. Syono & M.H. Manghnani, eds. AGU, Washington DC, 157–166.
- Zaug, J.M., Slutsky, L.J., Brown, J.M. (1994): Equilibrium properties and structural relaxation in methanol to 30.4 GPa. *J. Phys. Chem.*, **98**, 6008–6016.
- Zha, C.-S., Duffy, T.S., Downs, R.T., Mao, H.K., Hemley, R.J. (1996): Sound velocity and elasticity of single-crystal forsterite to 16 GPa. *J. Geophys. Res.*, **101**, 17535–17545.
- Zha, C.-S., Mao, H.-K., Hemley, R.J. (2000): Elasticity of MgO and a primary pressure scale to 55 GPa. *Proc. Nat. Acad. Sci.*, **97**, 13494–13499.

Received 28 August 2008

Modified version received 2 December 2008

Accepted 16 February 2009